

End-to-end Learning, with or without Labels

Corinne Jones, Vincent Roulet, Zaid Harchaoui

University of Washington
`{cjones6, vroulet, zaid}@uw.edu`

December 21, 2024

Abstract

We present an approach for end-to-end learning that allows one to jointly learn a feature representation from unlabeled data (with or without labeled data) and predict labels for unlabeled data. The feature representation is assumed to be specified in a differentiable programming framework, that is, as a parameterized mapping amenable to automatic differentiation. The proposed approach can be used with any amount of labeled and unlabeled data, gracefully adjusting to the amount of supervision. We provide experimental results illustrating the effectiveness of the approach.

1 Introduction

Deep networks trained end-to-end are now ubiquitous, being used for tasks ranging from lung cancer screening to music transcription to pose estimation (Ardila et al., 2019; Thickstun et al., 2018; Li et al., 2018). One frequent obstacle when considering new application domains is the need for these networks to be trained in a supervised manner on vast quantities of labeled data. Unfortunately, in many application domains only a small amount of labeled data can be collected or even exists. However, there often exist vast quantities of unlabeled data that are left untouched with a supervised training approach. Recent work as surveyed in (Oliver et al., 2018) exploits this unlabeled data in a variety of ways to learn feature representations, either with unsupervised or semi-supervised approaches.

Recently a number of papers have focused on *ad hoc* approaches using both labeled and unlabeled data in order to achieve the best possible performance in a common domain-specific task. Examples of such approaches include Deep Clustering (Caron et al., 2018) and TagLM (Peters et al., 2017), which achieved remarkable results in computer vision and in natural language processing, respectively. The impressive results obtained on common domain-specific tasks are often achieved thanks to a combination of interesting algorithms and clever tricks informed by expert domain knowledge. These, with the added recourse to industry-scale computing for parameter exploration, result in a lack of clarity of the overall objective actually considered and minimized. Furthermore, the connections with unsupervised learning objectives on the one hand and with supervised learning objectives on the other hand are often partial and unclear.

In this paper we propose a unified framework for end-to-end learning, applicable when there is only unlabeled data, or some unlabeled data and some labeled data, or only labeled data. The proposed framework motivates a precise objective function to be minimized. Furthermore the connections with classical unsupervised learning and supervised learning objectives are clear. Indeed, the objective naturally reduces to that of a clustering problem when we have no training set labels

and that of a classification problem when we have all of the training set labels. Moreover, due to its simplicity, this setup can be extended. For example, indirect constraints on the labels, such as requiring two unlabeled observations to have different labels, can be readily incorporated.

After reviewing related work on unsupervised and semi-supervised learning in Section 2, we present the framework in Section 3.1. We show that our proposed objective is smoother than a straightforward alternative. We address how to optimize the objective function in Section 3.2. Optimizing over the labels requires care, and for this we present a novel algorithm based on a convex relaxation of the problem. Finally, we demonstrate the proposed approach in Section 4, showing that our method, called XSDC, outperforms the supervised baseline.

2 Related Work

We survey recent approaches to end-to-end learning, that is, the joint learning of the parameterized mapping corresponding to the feature representation and the parameterized task-specific prediction mapping, in the presence of unlabeled data. These approaches relate to the areas of unsupervised and semi-supervised learning.

Unsupervised learning. Most unsupervised deep feature learning methods can be broadly classified into one of two categories: methods that optimize a surrogate loss, often based on known structure in the data; and methods that directly optimize a loss function of interest. Early examples of the former set of methods include auto-encoders, which attempt to reconstruct the input observations through a deep network (LeCun, 1987; Goodfellow et al., 2016). Other more recent examples attempt to approximate a kernel at each layer of a network (Bo et al., 2011; Mairal et al., 2014; Daniely et al., 2017). Most recently, many papers have been taking advantage of structure in the data. This includes training to distinguish between multiple views of images or patches and other images or patches (Wang and Gupta, 2015; Dosovitskiy et al., 2016; Sermanet et al., 2018; Bachman et al., 2019), learning to predict the relative location of patches in images (Doersch et al., 2015; Noroozi and Favaro, 2016), and predicting color from grayscale images (Zhang et al., 2016). It also includes learning to distinguish segments within time series or patches within images, or to predict future observations in time series (Hyvärinen and Morioka, 2016; van den Oord et al., 2018; Löwe et al., 2019). A downside to these latter approaches is the focus on achieving state-of-the-art results on domain-specific tasks in computer vision and signal processing at the expense of the conciseness of the formulation.

The second category of unsupervised methods typically alternately optimizes the parameters of the network and the labels or cluster assignments of the observations. In this thread, several papers alternate between obtaining assignments or soft assignments and optimizing the parameters of a loss function aimed at creating well-separated clusters (Xie et al., 2016; Yang et al., 2016; Ghasedi Dizaji et al., 2017; Häusser et al., 2017). In contrast, Bojanowski and Joulin (2017) randomly generate outputs and then alternately optimize over the parameters of the model and the assignment of labels to outputs. The most direct approach may be that of Caron et al. (2018), who alternately cluster the data to obtain pseudo-labels and take steps to optimize the multinomial logistic loss on the observations with the given pseudo-labels. A drawback of these approaches is the design of an *ad-hoc* objective not clearly related to objectives commonly used in unsupervised or supervised learning, or the combined use of two different objectives, one for optimizing the network and one for clustering. In this paper we build our formulation on a unified objective that encompasses learning with unlabeled data only, learning with labeled and unlabeled data, and learning with labeled data only.

Semi-supervised learning. We briefly summarize recent papers in semi-supervised learning. See the surveys of [Chapelle et al. \(2010\)](#) and [Oliver et al. \(2018\)](#) for a broader overview. Several recent methods create a semi-supervised algorithm by modifying a supervised algorithm. These modifications come in different flavors, such as adding a penalty to a supervised learning objective to encourage similar inputs to be close together in feature space ([Belkin et al., 2006](#); [Bachman et al., 2014](#); [Kamnitsas et al., 2018](#); [Iscen et al., 2019](#)), adding a penalty to encourage high-confidence outputs ([Grandvalet and Bengio, 2004](#)), or rounding outputs to obtain pseudo-labels ([Lee, 2013](#); [Berthelot et al., 2019](#)). Other approaches add a supervised loss to an unsupervised loss similar to those in the second category of unsupervised methods mentioned above ([Zhai et al., 2019](#)) or learn a feature representation in an unsupervised manner before fine-tuning with labeled data ([Wu et al., 2018](#)).

In contrast to these approaches, there is a set of principled approaches that do not learn a feature representation through a deep network but optimize over both the parameters of an affine functional classifier and the label assignments. Such approaches include constrained “forward prediction” using ridge regression or penalized multinomial logistic regression where the labels are also learned ([Bach and Harchaoui, 2007](#); [Joulin and Bach, 2012](#); [Flammarion et al., 2017](#)) and constrained “reverse prediction” using a k -means formulation or generalizations thereof ([Xu et al., 2009](#); [White and Schuurmans, 2012](#)). The advantage of the “forward prediction” objective introduced by [Bach and Harchaoui \(2007\)](#) is that it allows one to easily incorporate additional information about the clustering problem. Namely, it paved the way to several popular weakly supervised techniques developed by [Bojanowski et al. \(2014, 2015\)](#) and [Alayrac et al. \(2016\)](#) for computer vision problems.

Relation to existing methods. This work may be viewed as an extension of DIFFRAC ([Bach and Harchaoui, 2007](#)) for learning feature representations. As argued by [Jones et al. \(2019\)](#), a feature representation defined by a deep network can be related to an approximation of a feature map associated with a composition of kernels. From this viewpoint, the approach in this paper can also be interpreted as learning a kernel, i.e., a similarity measure, acting on pairs of examples.

In addition to using deep networks, we improve upon the work of [Bach and Harchaoui \(2007\)](#) by proposing a convex relaxation of the labeling subproblem. This relaxation allows us to handle several types of constraints on the labels. The proposed labeling procedure recovers the Sinkhorn-Knopp algorithm ([Sinkhorn and Knopp, 1967](#); [Peyré and Cuturi, 2019](#)) when there is no labeled data and the sizes of the clusters are assumed to be known.

3 Learning with any Level of Supervision

In this section we present the end-to-end learning framework, which takes advantage of any amount of labeled and unlabeled data.

3.1 Problem formulation

Consider observations $x_1, \dots, x_n \in \mathbb{R}^d$, each belonging to one of k classes. The class label corresponding to each x_i , denoted by $y_i^* \in \{0, 1\}^k$, may or may not be observed. We denote by \mathcal{S} the set of indices corresponding to the labeled data and by \mathcal{U} the set of indices corresponding to the unlabeled data. We aim to use both the labeled and unlabeled data to learn (1) the parameters V_ℓ at each layer $\ell = 1, 2, \dots, m$ of a differentiable deep network $\phi(\cdot; V) : \mathbb{R}^d \rightarrow \mathbb{R}^D$, where $V = \{V_1, \dots, V_m\}$; and (2) the parameters $W \in \mathbb{R}^{D \times k}$ and $b \in \mathbb{R}^k$ of a classifier on the output features $\phi(x_i; V)$, $i = 1, \dots, n$.

To this end, we consider solving the problem

$$\min_{Y \in \mathcal{C}, V, W, b} \frac{1}{n} \sum_{i=1}^n \ell(y_i, W^T \phi(x_i; V) + b) + \Omega(V, W),$$

where $\mathcal{C} = \{Y \in \{0, 1\}^{n \times k} : Y \mathbb{1}_k = 1, y_i = y_i^* \text{ for } i \in \mathcal{S}\}$ is the constraint set on the labels, $\ell(y, \hat{y}) = \|y - \hat{y}\|^2$ is the square loss, and $\Omega(V, W) := \alpha \sum_{j=1}^m \|V_j\|_F^2 + \lambda \|W\|_F^2$ contains the regularization terms. Here $\alpha \geq 0$ and $\lambda \geq 0$ are regularization parameters. Note that the label matrix Y is constrained so each point is assigned to a unique class.

The advantage of this objective is that it captures three regimes: the unsupervised regime, in which clustering is performed to learn the labels Y in addition to the network and classifier parameters V, W , and b ; the supervised regime, in which supervised training is performed to learn the parameters V, W , and b ; and the semi-supervised regime, in which a combination of clustering and supervised training are performed to learn the unknown labels y_i with $i \in \mathcal{U}$, in addition to the network and classifier parameters V, W , and b . Given an optimization algorithm for this objective, we may therefore proceed with training regardless of the amount of labeled data.

Avoiding trivial solutions. The above objective can lead to two different types of trivial solutions: one that maps all observations to the same embedding, i.e., $\phi(x_1; V) = \phi(x_2; V) = \dots = \phi(x_n; V)$; and one that assigns all observations to the same cluster, i.e., $y_1 = y_2 = \dots = y_n$. We avoid the first problem by subtracting the penalty $\rho \sum_{i=1}^n \|\phi(x_i; V) - \bar{\phi}\|_2^2$ on the squared norms of the centered embeddings, where $\bar{\phi} = 1/n \sum_{i=1}^n \phi(x_i; V)$. The second problem exists even when the network parameters V are fixed, as noted by [Bach and Harchaoui \(2007, Section 2.3\)](#). To avoid this behavior we add constraints enforcing that the clusters have a minimum and maximum size, i.e., $n_{\min} \mathbb{1}_k \leq Y^T \mathbb{1}_n \leq n_{\max} \mathbb{1}_k$ for some $n_{\max} \geq n_{\min}$.

Formally, we consider then the problem

$$\min_{Y \in \mathcal{C}', V, W, b} \frac{1}{n} \sum_{i=1}^n \ell(y_i, W^T \phi(x_i; V) + b) + \mathcal{R}(V, W) \quad (1)$$

where

$$\mathcal{R}(V, W) = \alpha \sum_{j=1}^m \|V_j\|_F^2 + \lambda \|W\|_F^2 - \rho \sum_{i=1}^n \|\phi(x_i; V) - \bar{\phi}\|_2^2$$

with $\rho, \alpha, \lambda \geq 0$. The constraint set for Y is now

$$\mathcal{C}' = \{Y \in \{0, 1\}^{n \times k} : Y \mathbb{1}_k = 1, y_i = y_i^* \text{ for } i \in \mathcal{S}, n_{\min} \mathbb{1}_k \leq Y^T \mathbb{1}_n \leq n_{\max} \mathbb{1}_k\}.$$

In the following we denote simply $\phi_i(V) = \phi(x_i; V)$ and $\Phi(V) = (\phi_1(V), \dots, \phi_n(V))^T$.

We shall in Section 3.2 present an algorithm to optimize this objective. We term the overall algorithm *XSDC* for “X-Supervised Discriminative Clustering”, where “X” can be “un”, “semi” or “_”, hence covering all cases.

Comparison to reverse prediction objective. The main component of our objective is regularized “forward prediction” least squares, which is given by $\|Y - \Phi(V)W - \mathbb{1}_n b^T\|_F^2/n + \lambda \|W\|_F^2$ for features $\Phi(V)$. We could alternatively consider “reverse prediction” least squares, which is given by $\|\Phi(V) - YW\|_F^2/n$ and is used in k -means. In both cases we would alternate between updating the parameters V and W and estimating the labels Y .

One way in which we can compare the quality of the objectives generated by these two options for learning a representation is via their smoothness properties, i.e., their Lipschitz-continuity and the Lipschitz-continuity of their gradients. These control the step sizes of optimization methods; see [Bertsekas \(2016\)](#) and [Nesterov \(2018\)](#) for a discussion of the interplay between smoothness properties and rates of convergence. We now proceed to show that when fixing the labels Y the forward prediction objective is smoother than the reverse prediction objective for appropriate choices of the regularization parameter λ .

For both objectives, we consider fixed labels $Y \in \{0, 1\}^{n \times k}$ with $Y \mathbb{1}_k = \mathbb{1}_n$. Moreover, for simplicity we will take $\alpha = \rho = 0$. Consider the “forward prediction” objective from (1). Define the centering matrix $\Pi_n = I_n - \mathbb{1}_n \mathbb{1}_n^T/n$. After minimizing over the bias b , the problem may be written as

$$\begin{aligned} \min_V F_f(\Phi(V)) &:= \min_{V,W} \frac{1}{n} \|\Pi_n[Y - \Phi(V)W]\|_F^2 + \lambda \|W\|_F^2 \\ &= \min_V \lambda \operatorname{tr}[YY^T A(\Phi(V))] , \end{aligned} \quad (2)$$

where $A(\Phi) = \Pi_n (\Pi_n \Phi \Phi^T \Pi_n + n\lambda I)^{-1} \Pi_n$.

The corresponding “reverse prediction” problem is given by

$$\begin{aligned} \min_V F_r(\Phi(V)) &:= \min_{V,W} \frac{1}{n} \|\Phi(V) - YW\|_F^2 \\ &= \min_V \frac{1}{n} \operatorname{tr}[(I - P_Y)\Phi(V)\Phi(V)^T] , \end{aligned}$$

where $P_Y = Y(Y^T Y)^{-1} Y^T$ is an orthonormal projector.

To compare the smoothness with respect to any matrix V_j , $j = 1, \dots, m$ it suffices to compute the smoothness with respect to Φ . The next two propositions do that and suggest that our “forward prediction” objective is generally smoother than the “backward prediction” objective. The proofs may be found in [Appendix A](#).

Proposition 1. *Let \mathcal{Z} be the set of all possible feature matrices $\Phi \in \mathbb{R}^{n \times D}$. Assume there exists $B \in \mathbb{R}$ such that for all $\Phi \in \mathcal{Z}$, $\|\Phi\|_2 \leq B$. Let n_{\max} be a bound on the maximum number of points in a cluster. Then the Lipschitz constants of F_f and F_r with respect to the spectral norm can be estimated by*

$$L_f := 2 \frac{n_{\max}}{\lambda n^2} B \quad \text{and} \quad L_r := \frac{2}{n} B ,$$

respectively. We therefore have $L_f \leq L_r$ for $\lambda \geq n_{\max}/n$.

Proposition 2. *Under the same assumption as Proposition 1, the Lipschitz constants of ∇F_f and ∇F_r with respect to the spectral norm can be estimated by*

$$\ell_f := \frac{8B^2 n_{\max}}{n^3 \lambda^2} + \frac{2n_{\max}}{n^2 \lambda} \quad \text{and} \quad \ell_r := \frac{2}{n} ,$$

respectively. We therefore have $\ell_f \leq \ell_r$ for $\lambda \geq n_{\max}/(2n) + \sqrt{n_{\max}^2 + 16B^2 n_{\max}}/(2n)$.

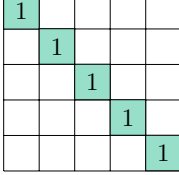
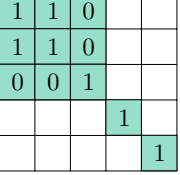
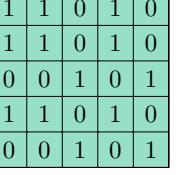
No supervision	Limited supervision	Full supervision
$M =$ 	$M =$ 	$M =$ 
$\min_{M,V} \text{Trace } MA(\Phi(V))$ <i>s.t.</i> $M \in \mathcal{C}'$	$\min_{M,V} \text{Trace } MA(\Phi(V))$ <i>s.t.</i> $M \in \mathcal{C}'$, M_{ij} fixed for $(i,j) \in \mathcal{K}$	$\min_V \text{Trace } MA(\Phi(V))$ <i>M fixed</i>

Figure 1: Example equivalence matrix M and objective function for varying levels of supervision. For simplicity we set $\alpha = \rho = 0$ in the objective functions.

3.2 Optimization

The algorithm XSDC that we propose to optimize the objective function (1) works on mini-batches. Below we will see that, with the square loss, we only ever need to work with the equivalence matrix $M := YY^T$ rather than the label matrix Y itself during training. Therefore, at each iteration we first optimize M for a mini-batch given fixed V, W , and b . Then we update W, b , and V for fixed M . Optimizing over M is the difficult part, and we propose a novel method for doing so. For the optimization over V, W , and b we use the Ultimate Layer Reversal Stochastic Gradient Optimization method (ULR-SGO) from [Jones et al. \(2019\)](#), which we review next.

Ultimate layer reversal. Rather than using stochastic gradient optimization to learn V, W , and b , we use the ULR-SGO method from [Jones et al. \(2019\)](#). It proceeds as follows. Denote the objective function (1) for fixed Y by $F_{\text{ulr}}(V, W, b)$. At each iteration, compute $\hat{F}_{\text{ulr}}(V) := \min_{W,b} F_{\text{ulr}}(V, W, b)$, rewriting the objective exclusively in terms of V . Then, using \hat{F}_{ulr} , update V by taking one gradient step.

As long as F_{ulr} is twice differentiable and F_{ulr} viewed as a function of W and b is strongly convex, gradient descent on this objective converges to a stationary point and the resultant ε -stationary points are ε -stationary points of the original problem. If $\hat{F}_{\text{ulr}}(V)$ is not available in closed form we may estimate it using a quadratic approximation of the loss around the current estimate of V . In addition, this method can also be applied on mini-batches and in the setting where V is constrained.

Optimizing using ULR-SGO has two main benefits. First, it was empirically shown by [Jones et al. \(2019\)](#) to converge faster than standard stochastic gradient optimization. Second, in the case of the square loss it allows us to work with the equivalence matrix $M = YY^T$ rather than the assignment matrix Y during the alternating optimization. To see this, observe that from Equation (2) we have

$$\hat{F}_{\text{ulr}}(V) = \lambda \text{tr}[MA(\Phi(V))] + R(V),$$

where A is defined as in Equation (2) and the regularization term is $R(V) := \alpha \sum_{j=1}^m \|V_j\|_F^2 - \rho \|\Pi_n \Phi(V)\|_F^2$. Since we only need to optimize over M we can avoid dealing with the problem of there being many solutions Y^* caused by the optimal objective value being the same if the columns of Y are permuted. In practice this means that we avoid performing an additional rounding step to obtain the assignment matrix. Figure 1 displays examples of the equivalence matrix M and the objective function in the cases of no labeled data, some labeled data, and fully labeled data.

Algorithm 1 Matrix Balancing

```

1: Inputs: Matrix  $A \in \mathbb{R}^{n \times n}$ 
2:           Matrix  $\hat{M} \in \{0, 1, ?\}^{n \times n}$  encoding known
3:           relations  $m_{i,j} \in \{0, 1\}$  with  $(i, j) \in \mathcal{K}$ 
4: Hyperparameters:
5: Minimum and maximum cluster sizes  $n_{\min}, n_{\max}$ ,
6: number of iterations  $T$ , entropic regularization  $\mu$ 
7: Initialize:  $\tilde{Q} = \mu^{-1}A - \log(\mathbb{1}_n \mathbb{1}_n^T/k)$ 
8:            $n_{\Delta} = (n_{\max} - n_{\min})/2$ 
9:            $n_{\Sigma} = (n_{\max} + n_{\min})/2$ 
10:           $u = v = \mathbb{1}_n$ 
11: for  $t = 1, \dots, T$  do
12:    $N_{ij} \leftarrow m_{ij}/(u_i v_j)$ ,  $(i, j) \in \mathcal{K}$ 
13:    $N_{ij} \leftarrow \exp(-\tilde{Q}_{ij})$ ,  $(i, j) \notin \mathcal{K}$ 
14:    $p_{v,i} \leftarrow \text{P}_{\mathcal{B}_{\infty}(n_{\Sigma}, n_{\Delta})}(N_{i,\cdot}^T v)$ ,  $i = 1, \dots, n$ 
15:    $u_i \leftarrow p_{v,i}/(N_{i,\cdot}^T v)$ ,  $i = 1, \dots, n$ 
16:    $p_{u,i} \leftarrow \text{P}_{\mathcal{B}_{\infty}(n_{\Sigma}, n_{\Delta})}(N_{\cdot,i}^T u)$ ,  $i = 1, \dots, n$ 
17:    $v_i \leftarrow p_{u,i}/(N_{\cdot,i}^T u)$ ,  $i = 1, \dots, n$ 
18: end for
19: Output:  $M = \text{diag}(u)N \text{diag}(v)$ 

```

Matrix balancing. Next, consider the objective function (1) when fixing V, W , and b and optimizing over only the equivalence matrix $M = YY^T$. As shown in Proposition 4 in Appendix B, this problem is NP-complete in general. Therefore, we consider a convex relaxation of it. We use an entropic regularizer $h(M) = \sum_{i,j=1}^n M_{ij} \log(M_{ij})$, which makes the objective strongly convex and enforces positivity of M . This regularizer appears in a Bregman divergence term $D_h(M; M_0) = h(M) - h(M_0) - \langle \nabla h(M_0), M - M_0 \rangle$, which can be used to ensure the output does not stray too far from an initial guess M_0 . Specifically, we consider the problem

$$\begin{aligned}
\min_M \quad & \frac{1}{2} \text{tr}(MA) + \mu D_h(M; M_0) \\
\text{subject to} \quad & M_{ij} = m_{ij} \quad \forall (i, j) \in \mathcal{K} \\
& n_{\min} \mathbb{1}_n \leq M \mathbb{1}_n \leq n_{\max} \mathbb{1}_n \\
& n_{\min} \mathbb{1}_n \leq M^T \mathbb{1}_n \leq n_{\max} \mathbb{1}_n ,
\end{aligned} \tag{3}$$

where the values m_{ij} for $i, j \in \mathcal{K} := (\mathcal{S} \times \mathcal{S}) \cup \{(1, 1), \dots, (n, n)\}$ represent the known entries of M .

Optimizing the dual of this problem via alternating minimization (see Appendix B), we obtain Algorithm 1. Note that in the case where the cluster sizes are predetermined and no labeled data exists, this reduces to the Sinkhorn-Knopp algorithm. The matrix balancing algorithm can be analyzed using the proof technique of Soules (1991). We detail in Appendix B the computation of the Jacobian driving the iteration process towards a fixed point. In practice we find that 10 steps of the alternating minimization suffice.

Overall algorithm. The overall XSDC algorithm for the case where some labeled data is present is summarized in Algorithm 2. The algorithm proceeds as follows. First, we initialize the pa-

Algorithm 2 XSDC (when some labeled data is present)

- 1: **Input:** Labeled data X_S, Y_S
- 2: Unlabeled data X_U
- 3: Randomly initialized network parameters $V^{(1)}$
- 4: Number of iterations T
- 5: **Initialize:**
 $V^{(1)}, W^{(1)}, b^{(1)} \leftarrow$ Optimize (1) over V, W, b using X_S, Y_S ,
starting from $V^{(1)}$
- 6: **for** $t = 1, \dots, T$ **do**
- 7: $X^{(t)}, Y^{(t)} \leftarrow$ Draw minibatch of samples
- 8: $M^{(t)} \leftarrow$ MatrixBalancing($A(\Phi(X^{(t)}; V^{(t)}))$, $Y^{(t)}Y^{(t)T}$)
- 9: $V^{(t+1)} \leftarrow$ ULR-SGO step($\Phi(X^{(t)}; V^{(t)})$, $M^{(t)}$, $V^{(t)}$)
- 10: **end for**
- 11: $\hat{Y}_U \leftarrow$ NearestNeighbor($\Phi(X; V^{(T)})$, Y_S)
- 12: $\hat{W}, \hat{b} \leftarrow$ RegLeastSquares(X ; $[Y_S, \hat{Y}_U]$)
- 13: **Output:** $\hat{Y}_U, V^{(T)}, \hat{W}, \hat{b}$

rameters V randomly and then optimize the objective on the labeled data to obtain initial estimates of V, W , and b . Next, we proceed to optimize using the labeled and unlabeled data together. At each iteration, we draw a mini-batch of n_b inputs $X^{(t)} = (x_1^{(t)}, \dots, x_{n_b}^{(t)})$ with corresponding labels $Y^{(t)}$ (some known, some unknown). We compute the output of the network $\Phi(X^{(t)}; V^{(t)}) = (\phi(x_1^{(t)}; V^{(t)}), \dots, \phi(x_{n_b}^{(t)}; V^{(t)}))^T$ and the corresponding matrix $A(\Phi(X^{(t)}; V^{(t)})) = \Pi_{n_b}(\Pi_{n_b} \Phi(X^{(t)}; V^{(t)}) \Phi(X^{(t)}; V^{(t)})^T \Pi_{n_b} + n_b \lambda \mathbf{I})^{-1} \Pi_{n_b}$. We then perform matrix balancing to obtain $M^{(t)}$. Fixing $M^{(t)}$, we then take a gradient step based on the ULR-SGO objective. At the end we obtain labels \hat{Y}_U for the unlabeled data using 1-nearest neighbor on the feature representations $\Phi(X; V)$. Finally, we estimate the parameters W and b by computing the solution to the least squares problem with X and $[Y_S, \hat{Y}_U]$. The algorithm for the case when no labeled data is present is similar; see Appendix C.2.

The XSDC algorithm has two significant benefits in addition to working with any amount of labeled data. First, learning the features does not require knowledge of the number of clusters. Instead, it requires only a bound on the fraction of points per cluster, for use in the matrix balancing. Specifying such a bound is easier than providing the number of clusters. The only time we must use knowledge of the number of clusters is when evaluating the performance of the learned features.

Second, the algorithm is trivially extendable to the case where we have additional must-link or must-not-link information related to the labels. For example, if we know observations i and j must not have the same label, we can encode that constraint in the above problem by adding (i, j) to \mathcal{K} and setting $m_{ij} = 0$. The algorithm itself is otherwise identical. This is an important extension for cases where labelers may not have been able to identify the correct label for an observation (e.g., “Welsh springer spaniel”) but could provide certain relevant label information (e.g., the label should be a dog breed).

4 Experiments

The framework we proposed may be applied to any amount of labeled and unlabeled data. In the experiments we illustrate how the proposed approach can be used for end-to-end learning when

few labels are known. Our goal is not to obtain state-of-the-art results in any specific application domain. Rather, we aim to show that our method is able to successfully leverage unlabeled data when labeled data is scarce. We show that when additional labeled data is unavailable but unlabeled data is plentiful we can typically use the unlabeled data to improve the classification accuracy.

We would expect our approach to improve if domain-specific tricks were used. However, exploring specialized versions of our algorithm for specific applications is beyond the scope of this paper. Instead, we focus on unifying learning with no labeled data, some labeled data, and fully labeled data in a single training objective. We do this in a domain-agnostic manner.

4.1 Choice of ϕ

One benefit of the XSDC algorithm is that it can learn a similarity measure for clustering. Typical clustering methods either do not transform the features or use a kernel-based method. However, clustering in the original feature space is often ineffective. Moreover, clustering using the Gram matrix on the inputs is infeasible when there are a large number of observations and ineffective when the kernel is improperly chosen (Perez-Cruz and Bousquet, 2004). In this work we therefore consider kernel networks for ϕ that are trained to approximate a kernel at each layer.

Many methods for approximating kernels exist, including random Fourier features and the Nyström method (Rahimi and Recht, 2007; Williams and Seeger, 2000; Mohri et al., 2012). Random Fourier features are data-independent and the parameters of the Nyström method are typically selected at random or via quantization (Oglic and Gärtner, 2017). We will instead learn the parameters of the Nyström method, similarly to Mairal (2016). The regularized Nyström method approximates a kernel k by computing the inner products of features $\phi(x)$ defined by $\phi(x) = (k(V^T V) + \epsilon I)^{-1/2} k(V^T x)$ for some small $\epsilon > 0$ where the matrix V contains the parameters.

We expect similar behavior for other kinds of networks, given observations made by Lee et al. (2018); Matthews et al. (2018); Belkin et al. (2018), and Jones et al. (2019).

4.2 Experimental details

Experimental setup. The experiments focus on four datasets: the vectorial datasets Gisette (Guyon et al., 2004) and MAGIC (Bock et al., 2004) and the image datasets MNIST (LeCun et al., 2001) and CIFAR-10 (Krizhevsky and Hinton, 2009). The sizes and dimensions of each dataset may be found in Table 1 in Appendix C. For more information regarding the dataset splits and how the data was transformed, see Appendix C.

The architectures we use in the experiments are kernel networks. For the vectorial datasets we use single-layer kernel networks (KNs) that approximate a Gaussian RBF kernel using the Nyström method. In contrast, for MNIST we use a convolutional kernel network (CKN) translation of LeNet-5 (LeCun et al., 2001; Jones et al., 2019) and for CIFAR-10 we use a CKN applied to the gradient map on the inputs (CKN-GM) (Mairal et al., 2014). For each of these networks we use 32 filters per layer for the hidden layers. These architectures and datasets were chosen because they represent a broad spectrum in terms of performance. For details on the parameter values and hold-out validation, see Appendix C. The hold-out validation is performed on the datasets for each quantity of labeled data but with a single random seed. The best parameters found are used for all other random seeds.

Training. The training is performed as follows. The network parameters are initialized by randomly sampling from the feature representations at each layer of the network. Then the network

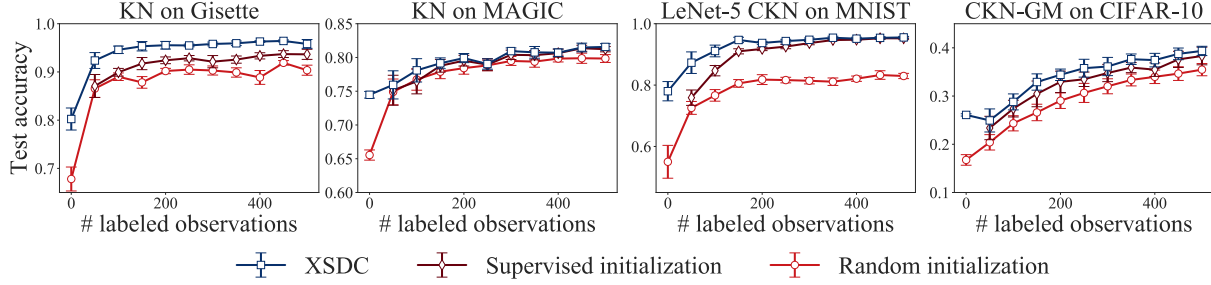


Figure 2: Average performance across 10 trials of XSDC when varying the quantity of labeled data. The error bars show one standard deviation from the mean.

is trained for 100 iterations using the labeled data. Finally, the network is trained using the ULR-SGO algorithm and matrix balancing on the labeled and unlabeled data for 400 iterations. Unless otherwise specified, $n_{\min} = n_{\max}$ in the matrix balancing, i.e., all classes are assumed to be equally represented within each mini-batch. We evaluate the performance of the learned representations every 10 iterations.

Code. The code for this project is written using Faiss, PyTorch, SciPy, and YesWeCKN (Johnson et al., 2017; Paszke et al., 2017; Virtanen et al., 2019; Jones et al., 2019). It may be found online at <https://github.com/cjones6/xsdc>.

4.3 Results

Improvement with unlabeled data. In the experiments we first compare the XSDC algorithm to two simple baselines: an initial supervised training of the classifier when the network has random weights (“random initialization”) and an initial supervised training of both the network and the classifier (“supervised initialization”). In the latter case the network is trained on only the labeled data. In both cases, when evaluating the performance the labels of the unlabeled data are first estimated using 1-nearest neighbor with the labeled data. The classifier is then trained on the labeled and unlabeled data. The reported accuracy of the supervised initialization is the test accuracy after 100 iterations. In contrast, the reported accuracy of XSDC when labeled data exists is the test accuracy observed at the iteration where the validation accuracy is highest. We report this value because the algorithm can overfit before 500 iterations. In the case where no labeled data exists we report the highest observed test accuracy. We performed 10 trials when varying the random seed and report the mean and standard deviation of the corresponding results.

We would expect that XSDC would provide an improvement over the supervised initialization when there are gains to be had from additional labeled data. Otherwise, we would expect training on additional unlabeled data to provide little to no benefit. This is what we see in Figure 2. Figure 2 compares the accuracy of the XSDC algorithm to the initializations as the quantity of labeled data varies. From all of the plots we can see that the performance of XSDC relative to the supervised baseline is much larger when the quantity of labeled data is smaller. With 50 labeled examples the accuracy on Gisette increases by 5% on average when using XSDC instead of the supervised baseline. On MAGIC the gain is more modest, at 1%. For MNIST the gain is 13%, while for CIFAR-10 it is 5%. In contrast, for 500 labeled observations XSDC outperforms the supervised baseline by 2% on Gisette but is only 0.3% better than the baseline on MAGIC. The latter results make sense since the increase in performance of the supervised initialization with the quantity of labeled data has started leveling off by then. On MNIST the improvement when there are 500 labeled observations

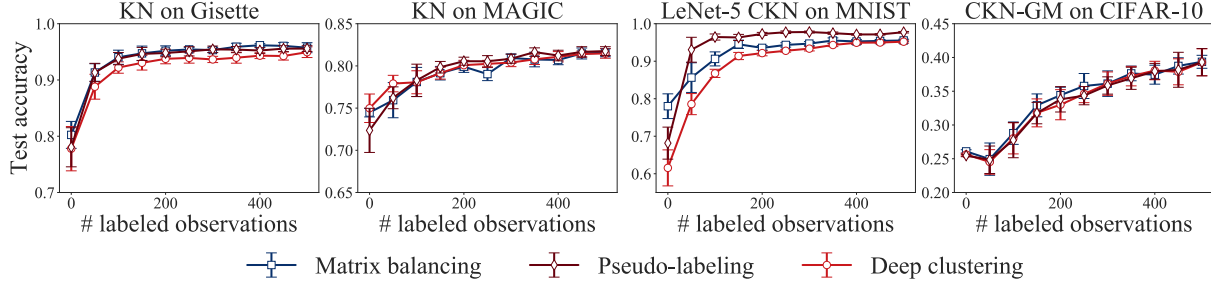


Figure 3: Average performance across 10 trials of XSDC with matrix balancing and two alternative labeling methods (pseudo-labeling and deep clustering) when varying the quantity of labeled data. The error bars show one standard deviation from the mean.

drops to 0.3%, while on CIFAR-10 it drops to 1.1%.

There are two other noteworthy aspects of Figure 2. First, it shows that XSDC can improve over the unsupervised initialization even in the case where there is no labeled data. The relative improvement in accuracy over the unsupervised baseline ranges from 14% on MAGIC to 56% on CIFAR-10 when no labeled data is present. Second, the standard error of the difference in the performance between the supervised baseline and XSDC tends to be larger when the gap in the performance between XSDC and the supervised baseline is larger, as expected. For example, on Gisette the standard error of the difference in the performance of XSDC and the supervised baseline is 1.6% in the case of 50 labeled observations, but only 0.9% in the case of 500 labeled observations.

We also visualize the results, examining the case where 50 images from MNIST are labeled. Figure 6 in Appendix D depicts the feature representations of the unlabeled data at various points of the training process. For each plot the feature representation was projected to 2-D using t-SNE (Van Der Maaten and Hinton, 2008). The observations are color-coded according to their true labels. For more details regarding the visualization, see Appendix D. Comparing Figures 6c and 6d, we can see that XSDC tends to increase the separation between clusters relative to the supervised initialization. The digits 4, 7, and 9 are a bit less separated. However, the digits 5 and 8 are each generally all in one cluster after running XSDC.

Comparison to alternative labeling methods. Next, we compare to two alternative labeling methods: pseudo-labeling (Lee, 2013) and deep clustering (Caron et al., 2018). Pseudo-labeling is a method designed to learn feature representations from labeled data and unlabeled data. Label assignment is performed by predicting labels from regression on the learned features. In contrast, deep clustering is a method designed to learn feature representations from unlabeled data and assign labels to unlabeled data. Label assignment is performed by k -means clustering with the learned features. Designing a variant working with both labeled data and unlabeled data was beyond the scope of Caron et al. (2018). See Appendix C.4 for how we adapted pseudo-labeling and deep clustering to the unsupervised setting and the semi-supervised setting, respectively.

Figure 3 displays results comparing the labeling method in XSDC (matrix balancing) to the labeling methods from pseudo-labeling and deep clustering in the case where some labeled data is present. From the plots we can see that the accuracy with matrix balancing and pseudo-labeling are only significantly different when training the LeNet-5 CKN on MNIST. However, both matrix balancing and pseudo-labeling typically outperform deep clustering when training the kernel network on Gisette and the LeNet-5 CKN on MNIST. On average, matrix balancing is 0.8-3% better than deep clustering when training the kernel network on Gisette and 0.3-21% better than deep clustering when training the LeNet-5 CKN on MNIST. These results suggest that for certain architectures

and datasets, using label information may be essential to achieving a performance close to the best possible one. On the other hand, the choice of how that label information is incorporated, whether it is by matrix balancing or pseudo-labeling, may matter less frequently in terms of the performance.

Improvement with additional constraints. As noted in Section 3.2, XSDC can seamlessly incorporate additional must-link and must-not-link constraints. To assess the benefit of adding such constraints, we provide additional experiments with LeNet-5 on MNIST. We consider two forms of additional constraints: (1) Must-not-link constraints derived from knowledge of whether or not each unlabeled observation was from class 4 or 9; and (2) Random correct must-link and must-not-link constraints among pairs of unlabeled observations and random correct must-not-link constraints between pairs of unlabeled and labeled observations. The pairs of classes in (1) were selected because they are frequently confused. This attempts to mimic a situation in which a labeler knows that an observation belongs to one of two classes, but is not sure which one. Each random constraint in (2) was added with probability 1/3, yielding approximately the same number of constraints as (1). See Appendix C.5 for additional details.

Figure 4b visualizes the feature representations resulting from constraints of the form (1) for the case of 50 labeled observations from MNIST. Examining this figure, we can see that the clusters are generally well-separated, including the bright green, light blue, and purple clusters, which correspond to the digits 4, 7, and 9, respectively. Visually, this is an improvement over the t-SNE projections when the additional constraints are not used (*cf.* Figure 4a).

Finally, Figure 7 in Appendix D displays results comparing the test accuracy on MNIST when including and not including the additional constraints on the labels. As expected, adding the additional constraints generally improves the performance. The addition of random correct constraints results in the best performance, likely because these provide more knowledge related to the difficult-to-distinguish classes.

Performance with unbalanced data. The XSDC algorithm can handle unbalanced datasets by changing the bounds on the cluster sizes in the matrix balancing algorithm. To present an example of how XSDC performs on unbalanced unlabeled data we again trained LeNet-5 on MNIST. We used 50 labeled observations, equally distributed across classes. For the unlabeled data we varied the fraction of labels 0-4 and the fraction of labels 5-9 between 5% and 95%. For training we use the hold-out validation set to determine the bounds on the cluster sizes.

The results are presented in Figure 7b in Appendix D. Training with XSDC on both the labeled and unlabeled data is nearly always better than training on the labeled data only (dashed curve). As expected, the performance tends to be better for more balanced data. The best accuracy was 85%, obtained with 40% 0-4's, while the worst accuracy was 64%, obtained with 95% 0-4's. In contrast, the accuracy when training on only the labeled data was 69%. These results suggest that as long as one believes that the unlabeled data is not extremely unbalanced, it could be beneficial to use it during training.

Sensitivity to hyperparameters. The XSDC algorithm generally has four or five hyperparameters to tune in the semi-supervised case (depending on the network). In order to assess the importance of these parameters, we perform a sensitivity analysis, again for LeNet-5 on MNIST with 50 labeled observations. Figure 8 in Appendix D displays the results when varying one parameter at a time, fixing the others to their values from cross-validation. From the plots we can see that the parameter that requires the most careful tuning in this setting is the semi-supervised learning rate.

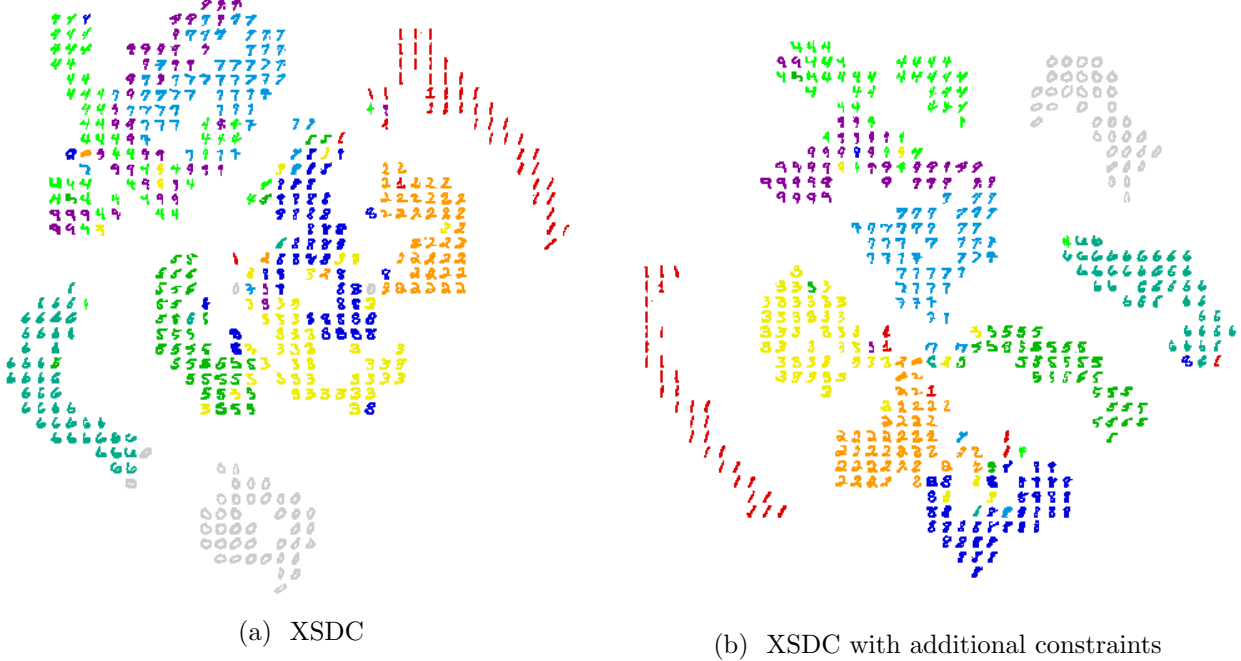


Figure 4: Visualizations of the unlabeled MNIST features obtained when training the LeNet-5 CKN with 50 labeled observations. The CKN features were projected to 2-D using t-SNE. The constraints used in (b) were derived from knowledge of whether the label for each unlabeled point lay in the set $\{4,9\}$.

The learning rate for the supervised initialization, along with the penalties on the centered features and classifier weights, just need to be sufficiently small.

5 Conclusion

In this work we presented a principled learning algorithm called XSDC that can be used on any amount of labeled and unlabeled data. In the special case of unsupervised learning the objective is a clustering objective in which the feature representation is also learned. In contrast, in the special case of supervised learning, the objective is a classification objective. We demonstrated the effectiveness of XSDC on four datasets, showing that when adding additional labeled data would help, substituting it with unlabeled data often yields large performance improvements.

Acknowledgements

The authors would like to gratefully acknowledge support from NSF CCF-1740551, NSF DMS-1810975, the program “Learning in Machines and Brains” of CIFAR, and faculty research awards. This work was first presented at the Women in Machine Learning Workshop in December 2019, for which the first author received travel funding from NSF IIS-1833154.

References

J.-B. Alayrac, P. Bojanowski, N. Agrawal, J. Sivic, I. Laptev, and S. Lacoste-Julien. Unsupervised learning from narrated instruction videos. In *Conference on Computer Vision and Pattern Recognition*, pages 4575–4583, 2016.

D. Ardila, A. P. Kiraly, S. Bharadwaj, B. Choi, J. J. Reicher, L. Peng, D. Tse, M. Etemadi, W. Ye, G. Corrado, D. P. Naidich, and S. Shetty. End-to-end lung cancer screening with three-dimensional deep learning on low-dose chest computed tomography. *Nature Medicine*, 2019.

F. R. Bach and Z. Harchaoui. DIFFRAC: a discriminative and flexible framework for clustering. In *Neural Information Processing Systems*, pages 49–56, 2007.

P. Bachman, O. Alsharif, and D. Precup. Learning with pseudo-ensembles. In *Advances in Neural Information Processing Systems*, pages 3365–3373, 2014.

P. Bachman, R. D. Hjelm, and W. Buchwalter. Learning representations by maximizing mutual information across views. *CoRR*, abs/1906.00910, 2019.

M. Belkin, P. Niyogi, and V. Sindhwani. Manifold regularization: A geometric framework for learning from labeled and unlabeled examples. *Journal of Machine Learning Research*, 7:2399–2434, 2006.

M. Belkin, S. Ma, and S. Mandal. To understand deep learning we need to understand kernel learning. In *International Conference on Machine Learning*, pages 540–548, 2018.

D. Berthelot, N. Carlini, I. Goodfellow, N. Papernot, A. Oliver, and C. Raffel. MixMatch: A holistic approach to semi-supervised learning. In *Advances in Neural Information Processing Systems*, pages 5050–5060, 2019.

D. P. Bertsekas. *Nonlinear programming*. Athena Scientific, 3rd edition, 2016.

L. Bo, K. Lai, X. Ren, and D. Fox. Object recognition with hierarchical kernel descriptors. In *Conference on Computer Vision and Pattern Recognition*, pages 1729–1736, 2011.

R. Bock, A. Chilingarian, M. Gaug, F. Hakl, T. Hengstebeck, M. Jirina, J. Klaschka, E. Kotrc, P. Savicky, S. Towers, A. Vaicius, and W. Wittek. Methods for multidimensional event classification: A case study using images from a Cherenkov gamma-ray telescope. *Nuclear Instruments and Methods in Physics Research Section A: Accelerators, Spectrometers, Detectors and Associated Equipment*, 516(2):511–528, 2004.

P. Bojanowski and A. Joulin. Unsupervised learning by predicting noise. In *International Conference on Machine Learning*, pages 517–526, 2017.

P. Bojanowski, R. Lajugie, F. Bach, I. Laptev, J. Ponce, C. Schmid, and J. Sivic. Weakly supervised action labeling in videos under ordering constraints. In *European Conference on Computer Vision*, pages 628–643, 2014.

P. Bojanowski, R. Lajugie, E. Grave, F. Bach, I. Laptev, J. Ponce, and C. Schmid. Weakly-supervised alignment of video with text. In *International Conference on Computer Vision*, pages 4462–4470, 2015.

M. Caron, P. Bojanowski, A. Joulin, and M. Douze. Deep clustering for unsupervised learning of visual features. In *European Conference on Computer Vision*, pages 139–156, 2018.

C.-C. Chang and C.-J. Lin. LIBSVM: A library for support vector machines. *ACM Transactions on Intelligent Systems and Technology*, 2:27:1–27:27, 2011.

O. Chapelle, B. Schlkopf, and A. Zien. *Semi-Supervised Learning*. The MIT Press, 1st edition, 2010.

A. Daniely, R. Frostig, V. Gupta, and Y. Singer. Random features for compositional kernels. *CoRR*, abs/1703.07872, 2017.

C. Doersch, A. Gupta, and A. A. Efros. Unsupervised visual representation learning by context prediction. In *International Conference on Computer Vision*, pages 1422–1430, 2015.

A. Dosovitskiy, P. Fischer, J. T. Springenberg, M. A. Riedmiller, and T. Brox. Discriminative unsupervised feature learning with exemplar convolutional neural networks. *IEEE Transactions on Pattern Analysis and Machine Intelligence*, 38(9):1734–1747, 2016.

N. Flammarion, B. Palaniappan, and F. Bach. Robust discriminative clustering with sparse regularizers. *Journal of Machine Learning Research*, 18:80:1–80:50, 2017.

K. Ghasedi Dizaji, A. Herandi, C. Deng, W. Cai, and H. Huang. Deep clustering via joint convolutional autoencoder embedding and relative entropy minimization. In *International Conference on Computer Vision*, pages 5747–5756, 2017.

I. J. Goodfellow, Y. Bengio, and A. C. Courville. *Deep Learning*. Adaptive computation and machine learning. MIT Press, 2016.

Y. Grandvalet and Y. Bengio. Semi-supervised learning by entropy minimization. In *Advances in Neural Information Processing Systems*, pages 529–536, 2004.

I. Guyon, S. R. Gunn, A. Ben-Hur, and G. Dror. Result analysis of the NIPS 2003 feature selection challenge. In *Advances in Neural Information Processing Systems*, pages 545–552, 2004.

P. Häusser, A. Mordvintsev, and D. Cremers. Learning by association - A versatile semi-supervised training method for neural networks. In *Conference on Computer Vision and Pattern Recognition*, pages 626–635, 2017.

A. Hyvärinen and H. Morioka. Unsupervised feature extraction by time-contrastive learning and nonlinear ICA. In *Advances in Neural Information Processing Systems*, pages 3765–3773, 2016.

A. Iscen, G. Tolias, Y. Avrithis, and O. Chum. Label propagation for deep semi-supervised learning. In *Conference on Computer Vision and Pattern Recognition*, pages 5070–5079, 2019.

J. Johnson, M. Douze, and H. Jégou. Billion-scale similarity search with GPUs. *CoRR*, abs/1702.08734, 2017.

C. Jones, V. Roulet, and Z. Harchaoui. Kernel-based translations of convolutional networks. *arXiv preprint arXiv:1903.08131*, 2019.

A. Joulin and F. R. Bach. A convex relaxation for weakly supervised classifiers. In *International Conference on Machine Learning*, 2012.

K. Kamnitsas, D. C. Castro, L. L. Folgoc, I. Walker, R. Tanno, D. Rueckert, B. Glocker, A. Criminisi, and A. V. Nori. Semi-supervised learning via compact latent space clustering. In *International Conference on Machine Learning*, pages 2464–2473, 2018.

R. M. Karp. Reducibility among combinatorial problems. *Kiberneticheskiu Sbornik. Novaya Seriya*, 12:16–38, 1975.

A. Krizhevsky and G. Hinton. Learning multiple layers of features from tiny images. Technical report, University of Toronto, 2009.

Y. LeCun. *Modeles connexionnistes de l'apprentissage*. PhD thesis, Université P. et M. Curie (Paris 6), June 1987.

Y. LeCun, L. Bottou, Y. Bengio, and P. Haffner. Gradient-based learning applied to document recognition. In *Intelligent Signal Processing*, pages 306–351. IEEE Press, 2001.

D.-H. Lee. Pseudo-label: The simple and efficient semi-supervised learning method for deep neural networks. In *International Conference on Machine Learning Workshop on Challenges in Representation Learning*, 2013.

J. Lee, Y. Bahri, R. Novak, S. S. Schoenholz, J. Pennington, and J. Sohl-Dickstein. Deep neural networks as Gaussian processes. In *International Conference on Learning Representations*, 2018.

Y. Li, G. Wang, X. Ji, Y. Xiang, and D. Fox. DeepIM: Deep iterative matching for 6D pose estimation. In *European Conference on Computer Vision*, pages 695–711, 2018.

S. Löwe, P. O'Connor, and B. Veeling. Putting an end to end-to-end: Gradient-isolated learning of representations. In *Advances in Neural Information Processing Systems*, pages 3033–3045, 2019.

J. Mairal. End-to-end kernel learning with supervised convolutional kernel networks. In *Advances in Neural Information Processing Systems*, pages 1399–1407, 2016.

J. Mairal, P. Koniusz, Z. Harchaoui, and C. Schmid. Convolutional kernel networks. In *Advances in Neural Information Processing Systems*, pages 2627–2635, 2014.

A. Matthews, J. Hron, M. Rowland, R. E. Turner, and Z. Ghahramani. Gaussian process behaviour in wide deep neural networks. In *International Conference on Learning Representations*, 2018.

M. Mohri, A. Rostamizadeh, and A. Talwalkar. *Foundations of Machine Learning*. Adaptive computation and machine learning. MIT Press, 2012.

Y. Nesterov. *Lectures on convex optimization*. Springer, 2nd edition, 2018.

M. Noroozi and P. Favaro. Unsupervised learning of visual representations by solving jigsaw puzzles. In *European Conference on Computer Vision*, pages 69–84, 2016.

D. Ong and T. Gärtner. Nyström method with kernel k-means++ samples as landmarks. In *International Conference on Machine Learning*, pages 2652–2660, 2017.

A. Oliver, A. Odena, C. A. Raffel, E. D. Cubuk, and I. J. Goodfellow. Realistic evaluation of deep semi-supervised learning algorithms. In *Advances in Neural Information Processing Systems*, pages 3239–3250, 2018.

A. Paszke, S. Gross, S. Chintala, G. Chanan, E. Yang, Z. DeVito, Z. Lin, A. Desmaison, L. Antiga, and A. Lerer. Automatic differentiation in PyTorch. In *Advances in Neural Information Processing Systems Workshop on Autodiff*, 2017.

F. Pedregosa, G. Varoquaux, A. Gramfort, V. Michel, B. Thirion, O. Grisel, M. Blondel, P. Prettenhofer, R. Weiss, V. Dubourg, J. Vanderplas, A. Passos, D. Cournapeau, M. Brucher, M. Perrot, and E. Duchesnay. Scikit-learn: Machine learning in Python. *Journal of Machine Learning Research*, 12:2825–2830, 2011.

F. Perez-Cruz and O. Bousquet. Kernel methods and their potential use in signal processing. *IEEE Signal Processing Magazine*, 21(3):57–65, May 2004.

M. E. Peters, W. Ammar, C. Bhagavatula, and R. Power. Semi-supervised sequence tagging with bidirectional language models. In *Association for Computational Linguistics, ACL 2017*, pages 1756–1765, 2017.

G. Peyré and M. Cuturi. Computational optimal transport. *Foundations and Trends in Machine Learning*, 11(5-6):355–607, 2019.

A. Rahimi and B. Recht. Random features for large-scale kernel machines. In *Advances in Neural Information Processing Systems*, pages 1177–1184, 2007.

P. Sermanet, C. Lynch, Y. Chebotar, J. Hsu, E. Jang, S. Schaal, and S. Levine. Time-contrastive networks: Self-supervised learning from video. In *International Conference on Robotics and Automation*, pages 1134–1141, 2018.

R. Sinkhorn and P. Knopp. Concerning nonnegative matrices and doubly stochastic matrices. *Pacific Journal of Mathematics*, 21:343–348, 1967.

G. W. Soules. The rate of convergence of Sinkhorn balancing. *Linear algebra and its applications*, 150:3–40, 1991.

J. Thickstun, Z. Harchaoui, D. P. Foster, and S. M. Kakade. Invariances and data augmentation for supervised music transcription. In *International Conference on Acoustics, Speech and Signal Processing*, pages 2241–2245, 2018.

A. van den Oord, Y. Li, and O. Vinyals. Representation learning with contrastive predictive coding. *CoRR*, abs/1807.03748, 2018.

L. Van Der Maaten and G. Hinton. Visualizing data using t-SNE. *Journal of Machine Learning Research*, 9:2579–2605, 2008.

P. Virtanen, R. Gommers, T. E. Oliphant, M. Haberland, T. Reddy, D. Cournapeau, E. Burovski, P. Peterson, W. Weckesser, J. Bright, S. van der Walt, M. Brett, J. Wilson, K. J. Millman, N. Mayorov, A. R. J. Nelson, E. Jones, R. Kern, E. Larson, C. J. Carey, I. Polat, Y. Feng, E. W. Moore, J. VanderPlas, D. Laxalde, J. Perktold, R. Cimrman, I. Henriksen, E. A. Quintero, C. R. Harris, A. M. Archibald, A. H. Ribeiro, F. Pedregosa, P. van Mulbregt, and Contributors. SciPy 1.0-Fundamental algorithms for scientific computing in Python. *CoRR*, abs/1907.10121, 2019.

X. Wang and A. Gupta. Unsupervised learning of visual representations using videos. In *International Conference on Computer Vision*, pages 2794–2802, 2015.

M. White and D. Schuurmans. Generalized optimal reverse prediction. In *International Conference on Artificial Intelligence and Statistics*, pages 1305–1313, 2012.

C. K. I. Williams and M. W. Seeger. Using the Nyström method to speed up kernel machines. In *Advances in Neural Information Processing Systems*, pages 682–688, 2000.

Z. Wu, Y. Xiong, S. X. Yu, and D. Lin. Unsupervised feature learning via non-parametric instance discrimination. In *Conference on Computer Vision and Pattern Recognition*, pages 3733–3742, 2018.

J. Xie, R. B. Girshick, and A. Farhadi. Unsupervised deep embedding for clustering analysis. In *International Conference on Machine Learning*, pages 478–487, 2016.

L. Xu, M. White, and D. Schuurmans. Optimal reverse prediction: a unified perspective on supervised, unsupervised and semi-supervised learning. In *International Conference on Machine Learning*, pages 1137–1144, 2009.

J. Yang, D. Parikh, and D. Batra. Joint unsupervised learning of deep representations and image clusters. In *Conference on Computer Vision and Pattern Recognition*, pages 5147–5156, 2016.

X. Zhai, A. Oliver, A. Kolesnikov, and L. Beyer. S^4L : Self-supervised semi-supervised learning. *CoRR*, abs/1905.03670, 2019.

R. Zhang, P. Isola, and A. A. Efros. Colorful image colorization. In *European Conference on Computer Vision*, pages 649–666, 2016.

A Smoothness of the Objective Function

In this appendix we estimate the smoothness constants for “forward prediction” regularized least squares and “backward prediction” least squares. Regularized forward prediction least squares learns to predict the label matrix Y from the features Φ :

$$\min_W \frac{1}{n} \|Y - \Phi W - \mathbb{1}_n b^T\|_F^2 + \lambda \|W\|_F^2$$

In contrast, reverse prediction least squares learns to predict the features Φ from the labels Y :

$$\min_W \frac{1}{n} \|\Phi - YW\|_F^2.$$

As noted by Xu et al. (2009), the solution of the forward prediction problem can be recovered from the solution of the reverse prediction problem as long as Φ is full rank.

Now we return to Proposition 1, which compared the Lipschitz constants of the two objectives, and provide its proof.

Proposition 1. *Let \mathcal{Z} be the set of all possible feature matrices $\Phi \in \mathbb{R}^{n \times D}$. Assume there exists $B \in \mathbb{R}$ such that for all $\Phi \in \mathcal{Z}$, $\|\Phi\|_2 \leq B$. Let n_{\max} be a bound on the maximum number of points in a cluster. Then the Lipschitz constants of F_f and F_r with respect to the spectral norm can be estimated by*

$$L_f := 2 \frac{n_{\max}}{\lambda n^2} B \quad \text{and} \quad L_r := \frac{2}{n} B,$$

respectively. We therefore have $L_f \leq L_r$ for $\lambda \geq n_{\max}/n$.

Proof. After minimizing in the classifier variable W , the forward prediction objective reads

$$F_f(\Phi) = \lambda \text{tr}[YY^T \Pi_n (\Pi_n \Phi \Phi^T \Pi_n + n\lambda \mathbf{I})^{-1} \Pi_n].$$

Define $G(\Phi) = (\Pi_n \Phi \Phi^T \Pi_n + n\lambda \mathbf{I}_n)^{-1}$. The gradient of F_f is then

$$\nabla F_f(\Phi) = -2\lambda \Pi_n G(\Phi) \Pi_n Y Y^T \Pi_n G(\Phi) \Pi_n \Phi.$$

Since $\|G(\Phi)\|_2 \leq 1/(n\lambda)$, $\|Y Y^T\|_2 \leq n_{\max}$, $\|\Pi_n\|_2 \leq 1$ and $\|G(\Phi) \Pi_n \Phi\|_2 \leq \|\Pi_n \Phi\|_2/(n\lambda)$, we obtain

$$\|\nabla F_f(\Phi)\|_2 \leq 2 \frac{n_{\max}}{\lambda n^2} B =: L_f.$$

Next, recall that the reverse prediction objective for fixed cluster assignments Y may be written as $F_r(\Phi) = \frac{1}{n} \text{tr}[(\mathbf{I} - P_Y) \Phi \Phi^T]$ where $P_Y = Y(Y^T Y)^{-1} Y^T$ is an orthonormal projector. Its gradient, $\nabla F_r(\Phi) = \frac{2}{n}(\mathbf{I} - P_Y)\Phi$, can therefore be bounded as

$$\|\nabla F_r(\Phi)\|_2 \leq \frac{2}{n} B =: L_r.$$

Hence, taking $\lambda \geq n_{\max}/n$, we have $\ell_f \leq \ell_r$. \square

Before moving on to the smoothness of the gradient we prove a lemma. The lemma estimates the Lipschitz constant of the gradient of the “forward prediction” objective function $F_f(\Phi)$ from Section 3.1.

Lemma 3. *Consider a feature matrix $\Phi \in \mathcal{Z}$ with $\Phi \in \mathbb{R}^{n \times D}$ and define the function $F_f : \mathbb{R}^{n \times D} \rightarrow \mathbb{R}$ by $F_f(\Phi) = \lambda \text{tr}[Y Y^T \Pi_n (\Pi_n \Phi \Phi^T \Pi_n + n\lambda \mathbf{I})^{-1} \Pi_n]$. Assume there exists B such that for all $\Phi \in \mathcal{Z}$, $\|\Phi\|_2 \leq B$. Then for all $\Phi_1, \Phi_2 \in \mathcal{Z}$,*

$$\|\nabla F_f(\Phi_1) - \nabla F_f(\Phi_2)\|_2 \leq \left(\frac{8B^2 n_{\max}}{n^3 \lambda^2} + \frac{2n_{\max}}{n^2 \lambda} \right) \|\Phi_1 - \Phi_2\|_2.$$

Hence, an upper bound on the Lipschitz constant of the gradient of $F_f(\Phi)$ is given by

$$\ell_f := \frac{8B^2 n_{\max}}{n^3 \lambda^2} + \frac{2n_{\max}}{n^2 \lambda}.$$

Proof. Note that the gradient of F_f is given by $\nabla F_f(\Phi) = -2\lambda \Pi_n G(\Phi) \Pi_n Y Y^T \Pi_n G(\Phi) \Pi_n \Phi$, where $G(\Phi) = (\Pi_n \Phi \Phi^T \Pi_n + n\lambda \mathbf{I})^{-1}$. Now let $\|\cdot\| = \|\cdot\|_2$ denote the spectral norm and observe that, using that $\|\Pi_n\| \leq 1$ since Π_n is a projection matrix,

$$\begin{aligned} & \frac{1}{2\lambda} \|\nabla F_f(\Phi_1) - \nabla F_f(\Phi_2)\| \\ &= \|\Pi_n G(\Phi_1) \Pi_n Y Y^T \Pi_n G(\Phi_1) \Pi_n \Phi_1 - \Pi_n G(\Phi_2) \Pi_n Y Y^T \Pi_n G(\Phi_2) \Pi_n \Phi_2\| \\ &\leq \underbrace{\|G(\Phi_1) \Pi_n Y Y^T \Pi_n G(\Phi_1) \Pi_n \Phi_1 - G(\Phi_2) \Pi_n Y Y^T \Pi_n G(\Phi_2) \Pi_n \Phi_1\|}_{(a)} \\ &\quad + \underbrace{\|G(\Phi_2) \Pi_n Y Y^T \Pi_n G(\Phi_2) \Pi_n \Phi_1 - G(\Phi_2) \Pi_n Y Y^T \Pi_n G(\Phi_2) \Pi_n \Phi_2\|}_{(b)}. \end{aligned}$$

First consider term (a). We have that

$$\begin{aligned} & \|G(\Phi_1) \Pi_n Y Y^T \Pi_n G(\Phi_1) \Pi_n \Phi_1 - G(\Phi_2) \Pi_n Y Y^T \Pi_n G(\Phi_2) \Pi_n \Phi_1\| \\ &= \|[G(\Phi_1) \Pi_n Y Y^T \Pi_n G(\Phi_1) - G(\Phi_2) \Pi_n Y Y^T \Pi_n G(\Phi_2)] \Pi_n \Phi_1\| \end{aligned}$$

$$\leq \underbrace{\|G(\Phi_1)\Pi_n YY^T \Pi_n G(\Phi_1) - G(\Phi_2)\Pi_n YY^T \Pi_n G(\Phi_2)\|}_{(c)} \|\Phi_1\|.$$

We may bound term (c) by

$$\begin{aligned} & \|G(\Phi_1)\Pi_n YY^T \Pi_n G(\Phi_1) - G(\Phi_2)\Pi_n YY^T \Pi_n G(\Phi_2)\| \\ & \leq \|G(\Phi_1)\Pi_n YY^T \Pi_n G(\Phi_1) - G(\Phi_1)\Pi_n YY^T \Pi_n G(\Phi_2)\| \\ & \quad + \|G(\Phi_1)\Pi_n YY^T \Pi_n G(\Phi_2) - G(\Phi_2)\Pi_n YY^T \Pi_n G(\Phi_2)\| \\ & \leq \|G(\Phi_1)\Pi_n YY^T \Pi_n\| \underbrace{\|G(\Phi_1) - G(\Phi_2)\|}_{(d)} + \|G(\Phi_2)\Pi_n YY^T \Pi_n\| \|G(\Phi_1) - G(\Phi_2)\|. \end{aligned}$$

Furthermore, we can bound term (d) via

$$\begin{aligned} \|G(\Phi_1) - G(\Phi_2)\| &= \|G(\Phi_1) [G(\Phi_1)^{-1} - G(\Phi_2)^{-1}] G(\Phi_2)\| \\ &\leq \|G(\Phi_1)\| \|G(\Phi_2)\| \underbrace{\|G(\Phi_1)^{-1} - G(\Phi_2)^{-1}\|}_{(e)} \end{aligned}$$

Finally, we can bound term (e) by

$$\begin{aligned} \|G(\Phi_1)^{-1} - G(\Phi_2)^{-1}\| &= \|\Pi_n \Phi_1 \Phi_1^T \Pi_n - \Pi_n \Phi_2 \Phi_2^T \Pi_n\| \\ &\leq \|\Phi_1 \Phi_1^T - \Phi_1 \Phi_2^T\| + \|\Phi_1 \Phi_2^T - \Phi_2 \Phi_2^T\| \\ &\leq \|\Phi_1\| \|\Phi_1 - \Phi_2\| + \|\Phi_2\| \|\Phi_1 - \Phi_2\|. \end{aligned}$$

Using this above, a bound on term (a) is thus

$$\begin{aligned} & \|G(\Phi_1)\Pi_n YY^T \Pi_n G(\Phi_1)\Pi_n \Phi_1 - G(\Phi_2)\Pi_n YY^T \Pi_n G(\Phi_2)\Pi_n \Phi_1\| \\ & \leq (\|G(\Phi_1)\Pi_n YY^T \Pi_n\| + \|G(\Phi_2)\Pi_n YY^T \Pi_n\|) \|G(\Phi_1)\| \|G(\Phi_2)\| (\|\Phi_1\| + \|\Phi_2\|) \|\Phi_1\| \|\Phi_1 - \Phi_2\|. \end{aligned}$$

Next, consider term (b). We have that

$$\begin{aligned} & \|G(\Phi_2)\Pi_n YY^T \Pi_n G(\Phi_2)\Pi_n \Phi_1 - G(\Phi_2)\Pi_n YY^T \Pi_n G(\Phi_2)\Pi_n \Phi_2\| \\ & \leq \|G(\Phi_2)\Pi_n YY^T \Pi_n G(\Phi_2)\| \|\Phi_1 - \Phi_2\|. \end{aligned}$$

Therefore, returning to the original quantity of interest, we have

$$\begin{aligned} & \frac{1}{2\lambda} \|\nabla F_f(\Phi_1) - \nabla F_f(\Phi_2)\| \\ & \leq \{ (\|G(\Phi_1)\Pi_n YY^T \Pi_n\| + \|G(\Phi_2)\Pi_n YY^T \Pi_n\|) \|G(\Phi_1)\| \|G(\Phi_2)\| (\|\Phi_1\| + \|\Phi_2\|) \|\Phi_1\| \\ & \quad + \|G(\Phi_2)\Pi_n YY^T \Pi_n G(\Phi_2)\| \} \times \|\Phi_1 - \Phi_2\|. \end{aligned}$$

We have $\|YY^T\|_2 \leq n_{\max}$, where n_{\max} is a bound on the maximum size of the clusters. Lastly, $\|G(\Phi_1)\|_2 \leq 1/(n\lambda)$ and $\|G(\Phi_2)\|_2 \leq 1/(n\lambda)$. Therefore, we have

$$\begin{aligned} \frac{1}{2\lambda} \|\nabla F_f(\Phi_1) - \nabla F_f(\Phi_2)\|_2 &\leq \left\{ \frac{2n_{\max}}{n\lambda} \left(\frac{1}{n\lambda} \right)^2 (2B)B + \frac{n_{\max}}{n^2\lambda^2} \right\} \|\Phi_1 - \Phi_2\|_2 \\ &= \left(\frac{4B^2 n_{\max}}{n^3 \lambda^3} + \frac{n_{\max}}{n^2 \lambda^2} \right) \|\Phi_1 - \Phi_2\|_2, \end{aligned}$$

and so an upper bound on the Lipschitz constant is given by

$$\ell_f := \left(\frac{8B^2 n_{\max}}{n^3 \lambda^2} + \frac{2n_{\max}}{n^2 \lambda} \right) .$$

□

Now we recall Proposition 2 from Section 3.1, which compared the Lipschitz constants of the gradients of the forward and reverse prediction objectives, and provide its proof.

Proposition 2. *Under the same assumption as Proposition 1, the Lipschitz constants of ∇F_f and ∇F_r with respect to the spectral norm can be estimated by*

$$\ell_f := \frac{8B^2 n_{\max}}{n^3 \lambda^2} + \frac{2n_{\max}}{n^2 \lambda} \quad \text{and} \quad \ell_r := \frac{2}{n} ,$$

respectively. We therefore have $\ell_f \leq \ell_r$ for $\lambda \geq n_{\max}/(2n) + \sqrt{n_{\max}^2 + 16B^2 n_{\max}}/(2n)$.

Proof. The gradient of F_f is given by $\nabla F_f(\Phi) = -2\lambda \Pi_n G(\Phi) \Pi_n Y \tilde{Y}^T \Pi_n G(\Phi) \Pi_n \Phi$. By Lemma 3 we have that

$$\|\nabla F_f(\Phi_1) - \nabla F_f(\Phi_2)\|_2 \leq \left(\frac{8B^2 n_{\max}}{n^3 \lambda^2} + \frac{2n_{\max}}{n^2 \lambda} \right) \|\Phi_1 - \Phi_2\|_2 .$$

Next, observe that the gradient of F_r is $\nabla F_r(\Phi) = \frac{2}{n}(\mathbf{I} - P_Y)\Phi$. Hence, we have

$$\|\nabla F_r(\Phi_1) - \nabla F_r(\Phi_2)\|_2 \leq \frac{2}{n} \|\Phi_1 - \Phi_2\|_2 .$$

For $\lambda \geq n_{\max}/(2n) + \sqrt{n_{\max}^2 + 16B^2 n_{\max}}/(2n)$, we therefore have $\ell_f \leq \ell_r$. □

B Solving the Label Assignment Problem

Now we address the problem of optimizing the labels for the unlabeled data. The following proposition shows that this discrete problem is in general NP-complete for $k > 2$.

Proposition 4. *Let $A \in \mathbb{R}^{n \times n}$. The label assignment problem*

$$\begin{aligned} & \min_Y \text{tr}(YY^T A) \\ & \text{s.t. } \sum_{j=1}^k Y_{ij} = 1, \quad i = 1, \dots, n \\ & \quad Y_{ij} \in \{0, 1\} \quad \forall i = 1, \dots, n, \quad j = 1, \dots, k \end{aligned}$$

is NP-complete for $k > 2$.

Proof. The proof will follow by showing that the k -coloring problem is a special case of the matrix balancing problem. Let G be an undirected, unweighted graph with no self-loops. Define $A \in \{0, 1\}^{n \times n}$ to be the adjacency matrix of G . Then G is k -colorable if and only if the following problem has minimum value zero:

$$\min_Y \sum_{j=1}^k \sum_{i, i' \in A} Y_{i,j} Y_{i',j}$$

$$\begin{aligned}
& s.t. \sum_{j=1}^k Y_{ij} = 1, \quad i = 1, \dots, n \\
& \quad Y_{ij} \in \{0, 1\} \quad \forall i = 1, \dots, n, \quad j = 1, \dots, k.
\end{aligned}$$

Noting that

$$\sum_{j=1}^k \sum_{i' \in A} Y_{i,j} Y_{i',j} = \text{tr}(YY^T A) ,$$

we may rewrite the above problem as

$$\begin{aligned}
& \min_Y \text{tr}(YY^T A) \\
& s.t. \sum_{j=1}^k Y_{ij} = 1, \quad \forall i = 1, \dots, n \\
& \quad Y_{ij} \in \{0, 1\} \quad \forall i = 1, \dots, n, \quad j = 1, \dots, k.
\end{aligned}$$

This is a special case of the matrix balancing problem, in which A is the adjacency matrix of a graph. Therefore, as the k -coloring problem is NP-complete for $k > 2$ (Karp, 1975), the label assignment problem with discrete assignments is also NP-complete for $k > 2$. \square

B.1 Matrix balancing algorithm

Due to the previous result we optimize a convex relaxation of the label assignment problem. Consider a similarity matrix $A \in \mathbb{R}^{n \times n}$ and a matrix $M \in \mathbb{R}^{n \times n}$ with some known entries m_{ij} whose indices lie in the set $\mathcal{K} \subset \{1, \dots, n\}^2$. Then, given minimum and maximum cluster sizes n_{\min} and n_{\max} , the problem we solve is

$$\begin{aligned}
& \min_{M \in \mathbb{R}^{n \times n}} \text{Tr}(M^T A) \\
& \text{subject to} \quad n_{\min} \mathbb{1} \leq M \mathbb{1} \leq n_{\max} \mathbb{1}, \quad n_{\min} \mathbb{1} \leq M^T \mathbb{1} \leq n_{\max} \mathbb{1}, \quad M \geq 0 \\
& \quad M_{ij} = m_{ij}, \quad (i, j) \in \mathcal{K} ,
\end{aligned}$$

where $\mathbb{1} = \mathbb{1}_n$ is the vector of ones in \mathbb{R}^n . The constants n_{\max} and n_{\min} are upper and lower bounds on the sizes of the clusters, respectively.

We consider an entropic regularization of the problem. Specifically, we use the entropic regularizer

$$h(M) = \sum_{ij} M_{ij} \log(M_{ij}) \quad \text{with} \quad \nabla h(M) = \mathbb{1} \mathbb{1}^T + \log(M) ,$$

where $\log(M)$ is understood to be applied element-wise. We make a proximal step from an initial guess M_0 by considering the Bregman divergence $D_h(M; M_0) = h(M) - h(M_0) - \langle \nabla h(M_0), M - M_0 \rangle = h(M) - \langle \mathbb{1} \mathbb{1}^T + \log(M_0), M \rangle + C$, where C is a constant. If $\mathcal{K} = \emptyset$ a feasible M_0 is given by $(M_0)_{ij} = 1/k$, where k is the number of clusters. Consider then the problem

$$\begin{aligned}
& \min_{M \in \mathbb{R}^{n \times n}} \text{Tr}(M^T A) + \mu D_h(M; M_0) \\
& \text{subject to} \quad n_{\min} \mathbb{1} \leq M \mathbb{1} \leq n_{\max} \mathbb{1}, \quad n_{\min} \mathbb{1} \leq M^T \mathbb{1} \leq n_{\max} \mathbb{1}, \quad M \geq 0
\end{aligned}$$

$$M_{ij} = m_{ij}, \quad (i, j) \in \mathcal{K} ,$$

which is equivalent to

$$\begin{aligned} & \min_{M \in \mathbb{R}^{n \times n}} \mathbf{Tr}(M^T Q) + \mu h(M) \\ \text{subject to} \quad & n_{\min} \mathbb{1} \leq M \mathbb{1} \leq n_{\max} \mathbb{1}, \quad n_{\min} \mathbb{1} \leq M^T \mathbb{1} \leq n_{\max} \mathbb{1}, \quad M \geq 0 \\ & M_{ij} = m_{ij}, \quad (i, j) \in \mathcal{K} . \end{aligned} \quad (4)$$

where $Q = A - \mu \mathbb{1} \mathbb{1}^T - \mu \log(M_0)$.

Dual problem. Considering the problem scaled by μ^{-1} and introducing Lagrange multipliers, we obtain

$$\begin{aligned} & \max_{\alpha \in \mathbb{R}^n, \beta \in \mathbb{R}^n, \gamma \in \mathbb{R}^n, \delta \in \mathbb{R}^n, \lambda \in \mathbb{R}^{|\mathcal{K}|}} \min_{M \in \mathbb{R}^{n \times n}} \mu^{-1} \mathbf{Tr}(M^T Q) + h(M) + \alpha^T (n_{\min} \mathbb{1} - M \mathbb{1}) - \beta^T (n_{\max} \mathbb{1} - M^T \mathbb{1}) \\ & \quad + \gamma^T (n_{\min} \mathbb{1} - M^T \mathbb{1}) - \delta^T (n_{\max} \mathbb{1} - M^T \mathbb{1}) \\ & \quad + \sum_{(i,j) \in \mathcal{K}} \lambda_{ij} (M_{ij} - m_{ij}) \\ \text{subject to} \quad & M \geq 0, \quad \alpha \geq 0, \quad \beta \geq 0, \quad \gamma \geq 0, \quad \delta \geq 0 . \end{aligned}$$

The minimum in M for $\alpha, \beta, \gamma, \delta$, and λ fixed can be computed analytically. It reads

$$M^* = \exp(-(\tilde{Q} + (\beta - \alpha) \mathbb{1}^T + \mathbb{1}(\delta - \gamma)^T + \Lambda)) ,$$

where $\tilde{Q} = \mu^{-1}Q + \mathbb{1} \mathbb{1}^T = \mu^{-1}A - \log(M_0)$ and $\Lambda = [\Lambda_{ij}]_{i,j=1}^n$ with $\Lambda_{ij} = \lambda_{ij}$ if $(i, j) \in \mathcal{K}$ and $\Lambda_{ij} = 0$ otherwise. The dual problem then reads

$$\begin{aligned} & \min_{\alpha \in \mathbb{R}^n, \beta \in \mathbb{R}^n, \gamma \in \mathbb{R}^n, \delta \in \mathbb{R}^n, \lambda \in \mathbb{R}^{|\mathcal{K}|}} \mathbb{1}^T \exp(-(\tilde{Q} + (\beta - \alpha) \mathbb{1}^T + \mathbb{1}(\delta - \gamma)^T + \Lambda)) \mathbb{1} \\ & \quad - n_{\min}(\alpha + \gamma)^T \mathbb{1} + n_{\max}(\beta + \delta)^T \mathbb{1} + \sum_{(i,j) \in \mathcal{K}} \lambda_{ij} m_{ij} \\ \text{subject to} \quad & \alpha \geq 0, \quad \beta \geq 0, \quad \gamma \geq 0, \quad \delta \geq 0 . \end{aligned}$$

Using the change of variables $a = \beta - \alpha$, $b = \beta + \alpha$, $c = \delta - \gamma$, $d = \delta + \gamma$, the dual problem is then

$$\begin{aligned} & \min_{a \in \mathbb{R}^n, b \in \mathbb{R}^n, c \in \mathbb{R}^n, d \in \mathbb{R}^n, \lambda \in \mathbb{R}^{|\mathcal{K}|}} \exp(-a)^T \exp(-(\tilde{Q} + \Lambda)) \exp(-c) \\ & \quad + \frac{n_{\max} - n_{\min}}{2} (b + d)^T \mathbb{1} + \frac{n_{\max} + n_{\min}}{2} (a + c)^T \mathbb{1} + \sum_{(i,j) \in \mathcal{K}} \lambda_{ij} m_{ij} \\ \text{subject to} \quad & b \geq |a|, \quad d \geq |c| . \end{aligned}$$

Minimization in b and d can be performed analytically (using $n_{\max} \geq n_{\min}$) such that the problem reads

$$\begin{aligned} & \min_{a \in \mathbb{R}^n, c \in \mathbb{R}^n, \lambda \in \mathbb{R}^{|\mathcal{K}|}} \exp(-a)^T \exp(-(\tilde{Q} + \Lambda)) \exp(-c) + n_{\Delta}(\|a\|_1 + \|c\|_1) + n_{\Sigma}(a + c)^T \mathbb{1} \\ & \quad + \sum_{(i,j) \in \mathcal{K}} \lambda_{ij} m_{ij} , \end{aligned} \quad (5)$$

where $n_{\Delta} = (n_{\max} - n_{\min})/2$ and $n_{\Sigma} = (n_{\max} + n_{\min})/2$.

Alternating minimization. We consider an alternating minimization scheme to solve (5).

Minimization in λ . Differentiating with respect to λ leads to

$$\exp(-\lambda_{ij}^*) = \exp(\tilde{Q}_{ij}) \exp(a_i^*) \exp(c_j^*) m_{ij} , \quad (i, j) \in \mathcal{K} .$$

Minimization in a . Minimization in a for c and λ fixed reads, denoting $x = \exp(-(\tilde{Q} + \Lambda^*)) \exp(-c^*)$,

$$\min_a \max_{\|\eta\|_\infty \leq 1} \exp(-a)^T x + a^T (n_\Sigma \mathbb{1} + n_\Delta \eta) .$$

Switching the max and min, the minimum in a for η fixed (which is always defined since $n_\Sigma \mathbb{1} + n_\Delta \eta \geq 0$ for $\|\eta\|_\infty \leq 1$) is given by

$$\exp(-a^*(\eta)_i) = (n_\Sigma + n_\Delta \eta_i) / x_i \quad i = 1, \dots, n .$$

Denoting $\theta = n_\Sigma \mathbb{1} + n_\Delta \eta$, the problem then reads

$$\max_{\|\theta - n_\Sigma \mathbb{1}\|_\infty \leq n_\Delta} \theta^T (\mathbb{1} + \log(x)) - \theta^T \log(\theta) .$$

Its minimum is reached at

$$\theta^* = P_{\mathcal{B}_\infty(n_\Sigma \mathbb{1}, n_\Delta)}(x) ,$$

where $P_{\mathcal{B}_\infty(n_\Sigma \mathbb{1}, n_\Delta)}$ is the projection on the infinity ball of radius n_Δ centered at $n_\Sigma \mathbb{1}$. We then get

$$\exp(-a_i^*) = P_{\mathcal{B}_\infty(n_\Sigma, n_\Delta)} \left(\exp[-(\tilde{Q} + \Lambda^*)]_{i,\cdot}^T \exp(-c^*) \right) / \left\{ \exp[-(\tilde{Q} + \Lambda^*)]_{i,\cdot}^T \exp(-c^*) \right\} .$$

Note that in the case where the clusters are constrained to all have the same size, i.e., $n_{\min} = n_{\max}$, the numerator reduces to n_Σ .

Minimization in c . Minimization in c is analogous and we get

$$\exp(-c^*) = P_{\mathcal{B}_\infty(n_\Sigma, n_\Delta)} \left(\exp[-(\tilde{Q} + \Lambda^*)]_{\cdot,i}^T \exp(-a^*) \right) / \left\{ \exp[-(\tilde{Q} + \Lambda^*)]_{\cdot,i}^T \exp(-a^*) \right\} .$$

Define $u = \exp(-a)$, $v = \exp(-c)$, and $N = \exp(-(\tilde{Q} + \Lambda))$. Given the above equations, the steps of the alternating minimization are given by:

$$\begin{aligned} N_{ij}^{(t+1)} &= m_{ij} / \left(u_i^{(t)} v_j^{(t)} \right) , & (i, j) \in \mathcal{K} \\ N_{ij}^{(t+1)} &= \exp(-\tilde{Q}_{ij}) , & (i, j) \notin \mathcal{K} \\ u_i^{(t+1)} &= P_{\mathcal{B}_\infty(n_\Sigma, n_\Delta)} \left(N_{i,\cdot}^{(t+1)T} v^{(t)} \right) / \left(N_{i,\cdot}^{(t+1)T} v^{(t)} \right) , & i = 1, \dots, n \\ v_i^{(t+1)} &= P_{\mathcal{B}_\infty(n_\Sigma, n_\Delta)} \left(N_{\cdot,i}^{(t+1)T} u^{(t+1)} \right) / \left(N_{\cdot,i}^{(t+1)T} u^{(t+1)} \right) , & i = 1, \dots, n . \end{aligned}$$

Assuming these converge to values N^* , u^* , and v^* , the final output is

$$M^* = \text{diag}(u^*) N^* \text{diag}(v^*) .$$

The algorithm is summarized in Algorithm 1.

B.2 Jacobian of the Sinkhorn iterations

Consider for $A \in \mathbb{R}^{n \times n}$ symmetric, the balancing problem

$$\begin{aligned} \min_{M \in \mathbb{R}^{n \times n}} \quad & \mathbf{Tr}(M^\top A) + \mu h(M) \\ \text{subject to} \quad & M\mathbb{1}_n = \alpha, M^\top \mathbb{1}_n = \beta, \end{aligned}$$

with $\alpha, \beta \in \mathbb{R}^n$, $h(M) = \sum_{ij} M_{ij} \log(M_{ij})$ and $\mathbb{1}_n$ denoting the vector of all ones in \mathbb{R}^n .

Its dual can be written

$$\min_{a, b \in \mathbb{R}^n} \exp(-a)^\top \exp(-\mu^{-1}A - \mathbb{1}_n \mathbb{1}_n^\top) \exp(-b) + a^\top \alpha + b^\top \beta,$$

and after a change of variables

$$\min_{u, v} u^\top Qv - \log(u)^\top \alpha - \log(v)^\top \beta, \quad (6)$$

where $Q = \exp(-\mu^{-1}A - \mathbb{1}_n \mathbb{1}_n^\top)$.

Alternating minimization on (6) reads, starting from $v_0 = \mathbb{1}_n$, for $t \geq 0$,

$$u_{t+1} = \alpha ./ (Qv_t), \quad v_{t+1} = \beta ./ (Q^\top u_{t+1}) \quad (7)$$

where $./$ denotes the element-wise division of two vectors. The iterations (7) can be written in matrix form as

$$Q_{t+1} = \tilde{\Pi}_\beta(\Pi_\alpha(Q_t)), \quad (8)$$

where for given vectors $\alpha, \beta \in \mathbb{R}^n$,

$$\Pi_\alpha(Q) = \text{diag}(\alpha ./ (Q\mathbb{1}_n))Q, \quad \tilde{\Pi}_\beta(Q) = Q \text{diag}(\beta ./ (Q^\top \mathbb{1}_n)) = (\Pi_\beta(Q^\top))^\top,$$

starting from $Q_0 = Q$ and we denoted for $x \in \mathbb{R}^n$, $\text{diag}(x) = \sum_{i=1}^n x_i e_i e_i^\top$, with e_i the i^{th} canonical vector in \mathbb{R}^n . We present the computation of the Jacobian of the iterative process around a fixed point in the following proposition. This Jacobian drives the application of the generalized Ostrowski theorem presented by [Soules \(1991\)](#).

Proposition 5. *For a given Q^* such that $\Pi_\alpha(Q^*) = Q^*$ and $\Pi_\beta(Q^*) = Q^*$, the Jacobian of the vectorized composition $\pi = \text{Vect} \circ \tilde{\Pi}_\beta \circ \Pi_\alpha \circ \text{Vect}^{-1}$ at $q^* = \text{Vect}(Q^*)$ reads*

$$\nabla \pi(q^*) = \sum_{i,j=1}^n (e_j e_j^\top - \mathbb{1}_n u_i^\top e_j e_j^\top) \otimes (e_i e_i^\top - e_i e_i^\top \mathbb{1}_n v_j^\top),$$

where $u_i = \frac{Q^\top e_i}{(Q^\top \mathbb{1}_n)_i}$, $v_j = \frac{Q e_j}{(Q^\top \mathbb{1}_n)_j}$.

Proof. For a matrix $Q \in \mathbb{R}^{n \times n}$, denote by $\text{Vect}(Q) \in \mathbb{R}^{n^2}$ the vectorized matrix (given by stacking the columns of Q). Denote by $\text{Vect}^{-1} : \mathbb{R}^{n^2} \rightarrow \mathbb{R}^{n \times n}$ the inverse operation such that $\text{Vect}^{-1}(\text{Vect}(Q)) = Q$. Denote by T the linear operator in \mathbb{R}^{n^2} such that for any $Q \in \mathbb{R}^{n \times n}$, $\text{Vect}(Q^\top) = T \text{Vect}(Q)$. We are interested in the vectorized formulation of Π_α, Π_β that read for $q \in \mathbb{R}^{n^2}$,

$$\pi_\alpha(q) = \text{Vect}(\Pi_\alpha(\text{Vect}^{-1}(q))) \quad \tilde{\pi}_\beta(q) = T\pi_\beta(Tq)$$

Precisely, denote $\pi = \tilde{\pi}_\beta \circ \pi_\alpha$. The iterations (8) then read

$$q_{t+1} = \pi(q_t).$$

Our assumption is that π has a fixed point q^* . We need then to show that π is Frechet differentiable at q^* and that $\rho(\nabla\pi(q^*)) < 1$. Since

$$\nabla\pi(q) = \nabla\pi_\alpha(q)\nabla\tilde{\pi}_\beta(\pi_\alpha(q)) ,$$

it boils down to analyzing that $\nabla\pi_\alpha(q)$ and $\nabla\tilde{\pi}_\beta(\pi_\alpha(q))$ are defined on q^* and that $\rho(\nabla\pi_\alpha(q)) < 1$ and $\rho(\nabla\tilde{\pi}_\beta(\pi_\alpha(q))) < 1$.

We begin by computing $\nabla\pi_\alpha(q)$. Note that $\nabla\tilde{\pi}_\beta(q) = T^\top \nabla\pi_\beta(q) T^\top$. In the following denote by $A \otimes B$ the Kronecker product of two matrices A, B and I_n the identity matrix in $\mathbb{R}^{n \times n}$. Recall the Kronecker formula for matrices with appropriate sizes: $\text{Vect}(AXB) = (B^\top \otimes A) \text{Vect}(X)$. We have for $q \in \mathbb{R}^{n^2}$, denoting $Q = \text{Vect}^{-1}(q)$, two formulations of π_α :

$$\begin{aligned}\pi_\alpha(q) &= (I_n \otimes \text{diag}(\alpha ./ (Q \mathbb{1}_n))) q \\ \pi_\alpha(q) &= (Q^\top \otimes I_n) \text{Vect}(\text{diag}(\alpha ./ (Q \mathbb{1}_n))) = (Q^\top \otimes I_n) E[\alpha ./ (\mathbb{1}_n^\top \otimes I_n) q]\end{aligned}$$

where $E = \sum_{i=1}^n (e_i \otimes e_i e_i^\top) \in \mathbb{R}^{n^2 \times n}$ such that $\text{Vect}(\text{diag}(x)) = Ex$ for $x \in \mathbb{R}^n$. We therefore get using the chain rule

$$\nabla\pi_\alpha(q) = \underbrace{(I_n \otimes \text{diag}(\alpha ./ (Q \mathbb{1}_n)))}_A + \underbrace{(\mathbb{1}_n \otimes I_n) \text{diag}(-\alpha ./ (Q \mathbb{1}_n) \cdot^2) E^\top (Q \otimes I_n)}_B ,$$

where we used that $f : x \rightarrow \alpha ./ x$ for $x \in \mathbb{R}^n$ has gradient $\nabla f(x) = \text{diag}(-\alpha ./ x \cdot^2)$ with \cdot^2 the element-wise application of the square operation and the gradient of $g : x \rightarrow Ax$ is $\nabla g(x) = A^\top$. Then we get

$$\begin{aligned}A &= \sum_{i=1}^n (I_n \otimes [\alpha_i / (Q \mathbb{1}_n)_i] e_i e_i^\top) = \sum_{i=1}^n [\alpha_i / (Q \mathbb{1}_n)_i] (I_n \otimes e_i e_i^\top) , \\ B &= -(\mathbb{1}_n \otimes I_n) \left(\sum_{j=1}^n [\alpha_j / (Q \mathbb{1}_n)_j^2] e_j e_j^\top \right) \left(\sum_{i=1}^n (e_i^\top \otimes e_i e_i^\top) (Q \otimes I_n) \right) \\ &= - \left(\sum_{j=1}^n [\alpha_j / (Q \mathbb{1}_n)_j^2] (\mathbb{1}_n \otimes e_j e_j^\top) \right) \left(\sum_{i=1}^n (e_i^\top Q \otimes e_i e_i^\top) \right) \\ &= - \sum_{i=1}^n [\alpha_i / (Q \mathbb{1}_n)_i^2] (\mathbb{1}_n (Q^\top e_i)^\top \otimes e_i e_i^\top) .\end{aligned}$$

Therefore, denoting $u_i = \frac{Q^\top e_i}{(Q \mathbb{1}_n)_i}$, we have

$$\nabla\pi_\alpha(q) = \sum_{i=1}^n \frac{\alpha_i}{(Q \mathbb{1}_n)_i} \left([I_n - \mathbb{1}_n u_i^\top] \otimes e_i e_i^\top \right) .$$

We get similarly, denoting $v_j = \frac{Q e_j}{(Q^\top \mathbb{1}_n)_j}$,

$$\nabla\pi_\beta(q) = \sum_{j=1}^n \frac{\beta_j}{(Q^\top \mathbb{1}_n)_j} T \left([I_n - \mathbb{1}_n v_j^\top] \otimes e_j e_j^\top \right) T$$

Table 1: Details regarding the datasets used in the experiments

Dataset	Training size	Validation size	Test size	Dimension	# Classes
CIFAR-10	40,000	10,000	10,000	3,072	10
Gisette	4,800	1,200	1,000	5,000	2
MAGIC	8,026	2,006	4,755	10	2
MNIST	50,000	10,000	10,000	784	10

$$= \sum_{j=1}^n \frac{\beta_j}{(Q^\top \mathbb{1}_n)_j} \left(e_j e_j^\top \otimes \left[\mathbb{I}_n - \mathbb{1}_n v_j^\top \right] \right) .$$

Therefore, denoting $\tilde{q} = \pi_\alpha(q)$, $\tilde{Q} = \text{Vect}^{-1}(\tilde{q})$ and $\tilde{v}_j = \frac{\tilde{Q} e_j}{(\tilde{Q}^\top \mathbb{1}_n)_j}$, we get

$$\nabla \pi(q) = \sum_{i,j=1}^n \frac{\alpha_i \beta_j}{(Q \mathbb{1}_n)_i (\tilde{Q}^\top \mathbb{1}_n)_j} (e_j e_j^\top - \mathbb{1}_n u_i^\top e_j e_j^\top) \otimes (e_i e_i^\top - e_i e_i^\top \mathbb{1}_n \tilde{v}_j^\top) .$$

In particular for q^* such that $\pi_\alpha(q^*) = q^*$ and $\pi_\beta(q^*) = q^*$, we get

$$\nabla \pi(q^*) = \sum_{i,j=1}^n (e_j e_j^\top - \mathbb{1}_n u_i^\top e_j e_j^\top) \otimes (e_i e_i^\top - e_i e_i^\top \mathbb{1}_n v_j^\top) .$$

□

C Additional Experimental Details

Here we provide additional details related to the datasets and the training.

C.1 Datasets

The details of the sizes and dimensions of each dataset we consider may be found in Table 1. For the MAGIC dataset, which does not have a train/test split, we randomly split the data 75%/25% into train/test sets. For Gisette, MAGIC, and CIFAR-10 we set aside 20% of the training set to use as a validation set, while for MNIST we set aside the standard 17%. For the imbalanced experiment we present on MNIST the size of the training dataset we use is always either 24,995 or 25,000, depending on rounding, with 50 labeled observations. Each class with labels 0-4 has the same number of unlabeled observations, and same for classes 5-9.

The datasets are transformed prior to usage as follows. Gisette is the scaled version found in the LibSVM database (Chang and Lin, 2011). MAGIC and MNIST are standardized. For CIFAR-10 we use the gradient map. As some of our experiments use the version of XSDC that assumes the classes are balanced, we randomly remove from the MAGIC dataset 4,223 observations in the training set with label 1.

C.2 XSDC with no labeled data

The XSDC algorithm for the purely unsupervised case is summarized in Algorithm 3. Aside from removing the supervised initialization step, the only difference lies in the estimation of \hat{Y}_U and the evaluation of the performance. Specifically, since we do not have any labeled data with which

Algorithm 3 XSDC (when no labeled data is present)

```
1: Input: Unlabeled data  $X_{\mathcal{U}}$ 
2:      Randomly initialized network parameters  $V^{(1)}$ 
3:      Number of iterations  $T$ 
4: for  $t = 1, \dots, T$  do
5:       $X^{(t)}, Y^{(t)} \leftarrow$  Draw minibatch of samples
6:       $M^{(t)} \leftarrow$  MatrixBalancing( $A(\Phi(X^{(t)}; V^{(t)})), Y^{(t)}Y^{(t)T}$ )
7:       $V^{(t+1)} \leftarrow$  ULR-SGO step( $\Phi(X^{(t)}; V^{(t)}), M^{(t)}, V^{(t)}$ )
8: end for
9:  $\hat{Y}_{\mathcal{U}} \leftarrow$  SpectralClustering( $M^{(T+1)}$ )
10:  $\hat{W}, \hat{b} \leftarrow$  RegLeastSquares( $X; \hat{Y}_{\mathcal{U}}$ )
11: Output:  $\hat{Y}_{\mathcal{U}}, V^{(T)}, \hat{W}, \hat{b}$ 
```

to perform nearest neighbor estimation, we instead use spectral clustering. Note that the cluster numbers output by spectral clustering do not necessarily map to the correct labels (e.g., cluster 0 might correspond to the label 1 rather than 0). Therefore, to evaluate the accuracy of the method we find the optimal relabeling of the classes that aligns with the true labels. We do so by solving a maximum weight matching problem with the Hungarian algorithm.

C.3 Parameters

The algorithm proposed in this paper and the models used require a large number of parameters to be set. Next we discuss the choices for these parameters.

Fixed parameters. The parameters that are fixed throughout the experiments and not validated are as follows. The number of filters in the networks is set to 32 and the network’s parameters V are initialized layer-wise with 32 feature maps drawn uniformly at random from the output of the previous layer. The networks use the Nyström method to approximate the kernel at each layer. The regularization in the Nyström approximation is set to 0.001, and 20 Newton iterations are used to compute the inverse square root of the Gram matrix on the parameters V_{ℓ} at each layer ℓ , as in [Jones et al. \(2019\)](#). The bandwidth is set to the median pairwise distance between the first 1000 observations for the single-layer networks. It is set to 0.6 for the convolutional networks. The batch size for both the labeled and unlabeled data is set to 4096 for Gisette and MAGIC and 1024 for MNIST and CIFAR-10 (due to GPU memory constraints). The features output by the network ϕ are centered and normalized so that on average they have unit ℓ_2 norm, as in [Mairal et al. \(2014\)](#). The initial training phase on just the labeled data is performed for 100 iterations, as the validation loss has typically started leveling off by 100 iterations. The entropic regularization parameter in the matrix balancing is set to the median absolute value of the entries in A . If this value results in divergence of the algorithm, it is multiplied by a factor of two until the algorithm converges. The value n_{Δ} is set to zero unless otherwise specified. The number of iterations of alternating minimization in the matrix balancing algorithm is set to 10. The number of nearest neighbors used for estimating the labels on the unlabeled data is set to 1.

Hold-out validation. Due to the large number of hyperparameters, we tune them sequentially as follows when labeled data, and hence a labeled validation set, exists. First, we tune the penalty λ on the classifier weights over the values 2^i for $i = -40, -39, \dots, 0$. To do so, we train the classifier

on only the labeled data using the initial random network parameters. We then re-cross-validate this value every 100 iterations. Next, we tune the learning rate for the labeled data. For the modest values of $\alpha = \rho = 2^{-4}$ we validate the fixed learning rate for the labeled data over the values 2^i for $i = -10, -9, \dots, 5$. To evaluate the performance the labels for the unlabeled data are estimated using 1-nearest neighbor. The labeled and unlabeled data are then used to train the classifier used to compute the performance. For the imbalanced experiments on MNIST only we then tune the minimum and maximum size of the classes over the values $0.01b, 0.02b, \dots, 0.2b$, where b is the batch size (fixing the semi-supervised learning rate to 2^{-5}). For all other experiments we fix these values to b/k , where k is the number of classes in the dataset. We then tune the semi-supervised learning rate, again over the values 2^i for $i = -10, -9, \dots, 5$. Following this, we validate ρ over the values 2^i for $i = -10, -9, \dots, 10$. For the single-layer networks we then tune α over the values 2^i for $i = -10, -9, \dots, 10$. For the convolutional networks we do not penalize the filters since they are constrained to lie on the sphere.

When no labeled data exists we consider the hyperparameters in the same manner as during the hold-out validation. First we consider the values 2^i for $i = -10, -9, \dots, 5$ for the semi-supervised learning rate. Next we consider the values 2^i for $i = -40, -39, \dots, 0$ for λ . We then consider the values 2^i for $i = -10, -9, \dots, 10$ for ρ . Finally, if applicable, we consider the values 2^i for $i = -10, -9, \dots, 10$ for α . We report the best performance observed on the test set. Developing a method for tuning the hyperparameters on an unlabeled validation set is left for future work.

C.4 Training with competing labeling methods

In the comparisons we substitute our matrix balancing method with alternative labeling methods and retain the remainder of the XSDC algorithm. The pseudo-labeling code is our own, but we used code from [Caron et al. \(2018\)](#) to implement the k -means version of deep clustering.¹ Two important details regarding the implementations are as follows. First, for pseudo-labeling when some of the data is labeled we estimate W and b based on the labeled data in the current mini-batch, as that is what is done in XSDC. When labeled data is not present we estimate W and b based on the cluster assignments for the entire dataset. Second, for deep clustering we modify the dimension of the dimensionality reduction. In the original implementation the authors performed PCA, reducing the dimensionality of the features output by the network to 256. As the features output by the networks we consider have dimension less than 256, we instead keep the fewest number of components that account for 95% of the variance.

We perform the parameter tuning as follows. First, we follow the tuning procedure as detailed in Section C.3. For pseudo-labeling there are no additional parameters to tune. However, for deep clustering there are two additional parameters to tune: the number of clusters in k -means and the number of iterations between cluster updates. During the initial parameter tuning stage these parameters are set to the true number of clusters k , and 50 iterations, respectively. Afterward we tune these two remaining parameters sequentially. We first tune the number of clusters over the values $k, 2k, 4k, 8k, 16k, 32k$ where k is the true number of clusters. We then tune the number of iterations between cluster updates over the values 10, 25, 50, 100.

C.5 Additional constraints

In one set of experiments we examine the effect of adding additional constraints. We consider two types of constraints: (1) Constraints based on knowledge of whether the label was in the set $\{4, 9\}$ or not; and (2) Random correct must-link and must-not-link constraints among pairs of unlabeled

¹<https://github.com/facebookresearch/deepcluster>

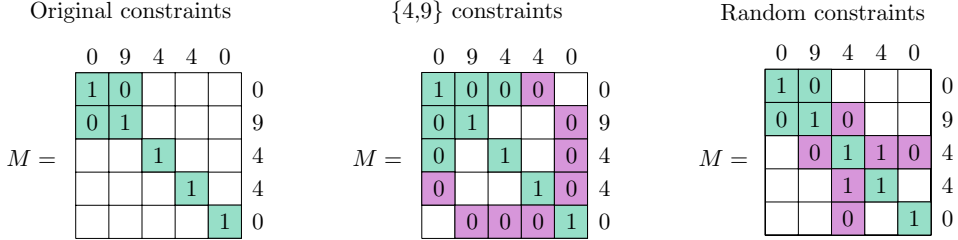


Figure 5: Illustration of the kinds of additional constraints that were added. Green denotes the original constraints while purple denotes the constraints that were added. The numbers outside of the grids denote the true labels.

observations and random correct must-not-link constraints between pairs of unlabeled and labeled observations.

The two types of constraints are illustrated in Figure 5. Each grid point (i, j) , if filled, denotes whether observations i and j have the same label (1) or not (0). The true labels are the values outside of the grids. Green backgrounds correspond to knowing the labels corresponding to (i, j) . Purple backgrounds denote the additional known constraints. The left-most panel gives an example of an initial matrix M in which the labels corresponding to the first two observations are known (0 and 9). The second panel shows the entries we can fill in once we know whether each observation belongs to the set $\{4, 9\}$. Finally, the third panel shows random correct constraints. The constraint at entry $(2, 3)$ is a must-not-link constraint, whereas the constraint at entry $(3, 4)$ is a must-link constraint.

D Additional Experimental Results

In this section we present additional experimental results that expand upon those presented in Section 4.

Visualization of feature representations. Figure 6 visualizes the feature representations of unlabeled MNIST digits at different points in the training process. In each case the features were projected to 2-D with the Scikit-Learn (Pedregosa et al., 2011) implementation of t-SNE (Van Der Maaten and Hinton, 2008). Based on these t-SNE representations, the plots were then produced. The code to produce the plots was adapted from Andrej Karpathy’s Matlab code.² It first scales the t-SNE representations so they all lie in $[0, 1]^2$ and creates an evenly-spaced 40×40 grid over $[0, 1]^2$. Then, for each square in the grid, it checks whether any image’s t-SNE representation lies in that square. If any such images exist, it chooses one at random and displays the original image in that square. The images are then color-coded according to the ground-truth labels.

The batch size used to produce the t-SNE representations and the corresponding plots was 4096. The default parameters were used for generating the t-SNE representations. We created each plot with 20 random initializations and present the ones that visually appeared to be the best.

Figure 6a visualizes the raw digits. By “raw” we mean that the digits were not input into the network; they were only standardized before applying t-SNE. Comparing this figure with Figure 6b, which visualizes the feature representations from the network with randomly initialized filters, we can see that in both plots the 4’s and 9’s are mixed together. Furthermore, the 5’s are split into two

²<https://cs.stanford.edu/people/karpathy/cnnembed/>

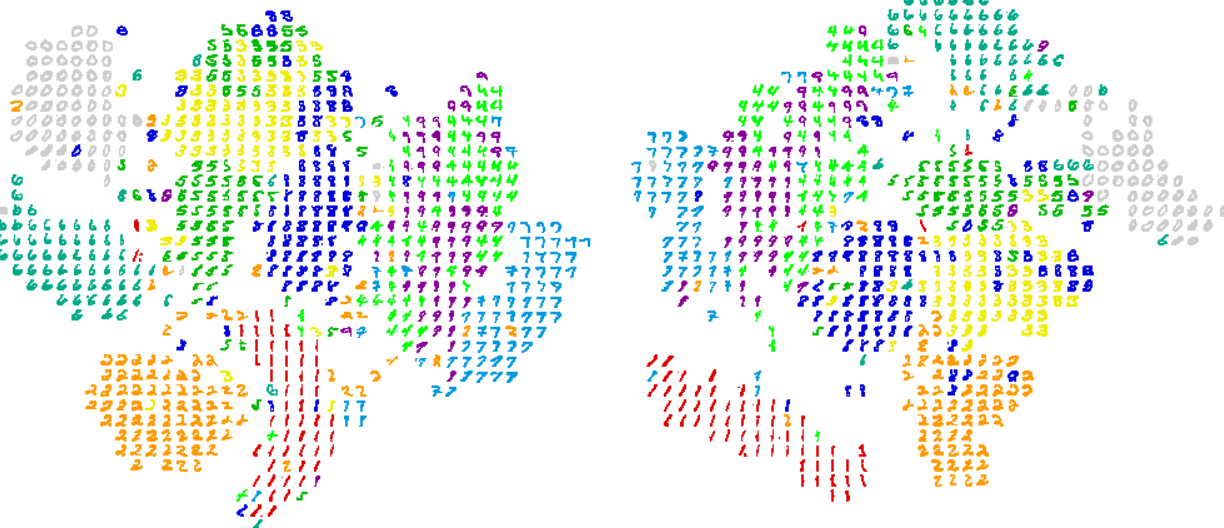
parts in Figure 6a. Figure 6c depicts the feature representations after the supervised initialization. Figure 6c improves upon 6b because the 4’s and 9’s are better-separated. However, the 5’s have once again been split into two parts. Finally, Figure 6d depicts the features representations after running XSDC. Comparing Figures 6c and 6d, we can see that XSDC tends to separate the clusters relative to the supervised initialization. While the 5’s and 8’s are generally all in one cluster after running XSDC, the 4’s, 7’s, and 9’s are a bit less separated.

Effect of additional constraints. Next, Figure 7 compares the test accuracy of the LeNet-5 CKN on MNIST when adding additional constraints. As explained in Section 4, we consider two types of additional constraints. The first type of constraints are generated based on knowledge of whether each unlabeled point has a label in the set $\{4, 9\}$ or not. The second type of constraints is randomly generated constraints with approximately the same number of known entries in the adjacency matrix M as for the first type. We can see that both types of additional constraints generally improve the performance of the method. The largest gap occurs when there are 50 labeled observations, as expected. There the accuracies on MNIST when using the additional $\{4, 9\}$ constraints and the random constraints are 1% better and 5% better, respectively, than without them. This gap shrinks to 0.03% and 0.8% at 500 observations. As noted in Section 4, it is likely that the better performance with the random constraints than with the $\{4, 9\}$ constraints is because the former provide more information to be able to distinguish between labels for often-confused classes. Note that the performance with the $\{4, 9\}$ constraints at 150 labels is worse than without the constraints. This is probably because the hold-out validation overfit on the validation set.

Effect of unbalanced unlabeled data. Figure 7b displays the accuracy of the LeNet-5 CKN on MNIST when 50 observations are labeled and the unlabeled data is unbalanced. To make the unlabeled data unbalanced we vary the fraction of the labels $\{0, 1, 2, 3, 4\}$ and the fraction of the labels $\{5, 6, 7, 8, 9\}$. Within each category 0-4 all of the labels are equally represented, and similarly for 5-9. The imbalance parameter in the plot denotes the fraction of the labels that are from the set $\{0, 1, 2, 3, 4\}$.

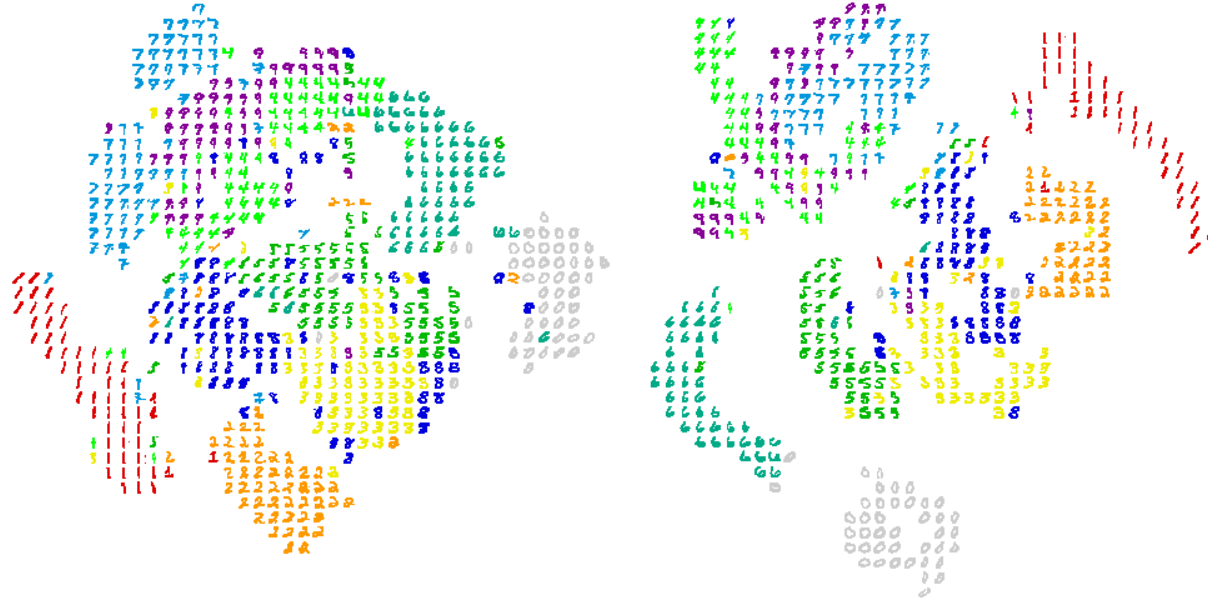
The performance is generally better when the data is closer to being balanced, as expected. The only time training with the unbalanced data is significantly worse than training on only the labeled data is when 95% of the unlabeled data is comprised of images of the digits 0-4. At that point the accuracy is 5% below the purely supervised performance.

Sensitivity analysis. Finally, we perform a sensitivity analysis of the hyperparameters that are tuned via cross-validation. To be consistent with the other experiments, the setting we choose is when training a LeNet-5 CKN on MNIST with 50 labels. For this architecture the parameters we cross-validate over are the learning rates for the supervised initialization and semi-supervised learning and the penalties on the centered features and classifier weights. Here we vary one parameter at a time, fixing all others to their values obtained from cross-validation (which were 2^{-7} and 2^{-6} for the learning rates of the supervised initialization and semi-supervised learning, respectively, and 2^{-5} for the penalty on the centered features. The penalty on the classifier weights was cross-validated every 100 iterations.). We see that the most important parameter to tune is the semi-supervised learning rate. The other parameters only have a noticeable detrimental effect if they are too large.



(a) Raw

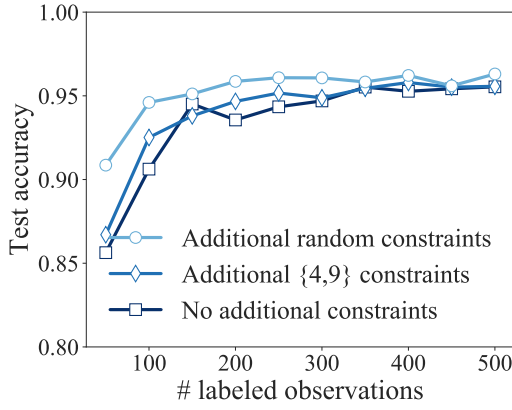
(b) Unsupervised initialization



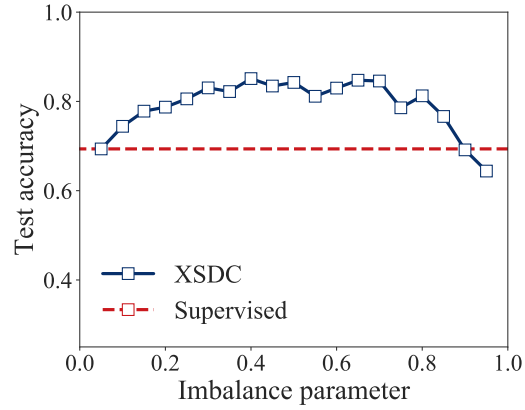
(c) Supervised initialization

(d) XSDC

Figure 6: Visualizations of the unlabeled MNIST features obtained when training the LeNet-5 CKN with 50 labeled observations (where applicable). The CKN features were projected to 2-D using t-SNE. The features were obtained at different stages, as indicated in the sub-captions.



(a) Effect of additional constraints



(b) Effect of unbalanced data

Figure 7: Average accuracy across 10 trials of XSDC after training a LeNet-5 CKN on MNIST when adding additional constraints and varying the fraction of labeled data (left) and when varying the balance of the unlabeled data (right). The “additional $\{4,9\}$ constraints” in (a) are derived from knowledge of whether the label for each unlabeled point lies in the set $\{4,9\}$. The imbalance parameter in (b) denotes the fraction of the labels that are from the set $\{0, 1, 2, 3, 4\}$. All classes in the set $\{0, 1, 2, 3, 4\}$ are equally represented, and similarly for $\{5, 6, 7, 8, 9\}$.

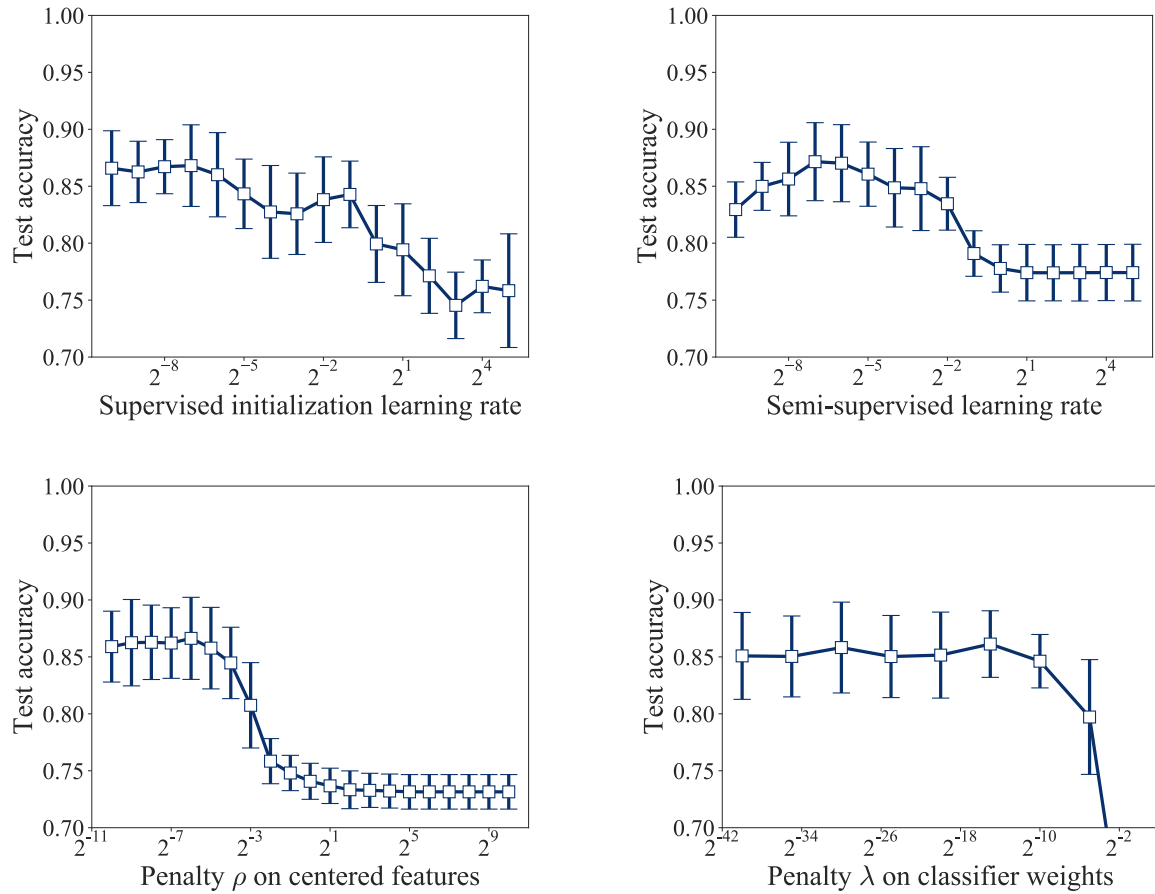


Figure 8: Sensitivity analysis of the hyperparameters tuned during cross-validation when using XSDC to train a LeNet-5 CKN on MNIST with 50 labeled observations.